applied sciences

MDPI

Review

Advances in Evaluation Methods for Artificial Fracture Networks in Shale Gas Horizontal Wells

Hang Yuan [1,2], Yuping Sun [2,3,*], Wei Xiong [1,2,3], Wente Niu [4], Zejun Tang [1] and Yong Li [1]

[1] Institute of Porous Flow and Fluid Mechanics, University of Chinese Academy of Sciences, Beijing 101400, China; yuanhang22@mails.ucas.ac.cn (H.Y.); xiongwei69@petrochina.com.cn (W.X.); tangzejun22@mails.ucas.ac.cn (Z.T.); liyong233@mails.ucas.ac.cn (Y.L.)
[2] National Energy Shale Gas R&D (Experimental) Center, Langfang 065007, China
[3] Research Institute of Petroleum Exploration and Development, Beijing 100089, China
[4] Department of Petroleum Engineering, School of Vehicle and Energy, Yanshan University, Qinhuangdao 066000, China; niuwente19@mails.ucas.edu.cn
* Correspondence: sunyuping01@petrochina.com.cn

Abstract

In recent years, the accurate evaluation of artificial fracture networks has become a key challenge in enhancing the effectiveness of reservoir stimulation in shale gas development. This paper systematically reviews the research progress on evaluation methods for artificial fracture networks in shale gas horizontal wells, covering two major technical systems: direct monitoring and dynamic inversion. Direct monitoring methods focus on technologies such as microseismic monitoring, tracers, wide-field electromagnetic methods, and distributed fiber optics. Dynamic inversion methods utilize data from fracturing construction curves, shut-in water hammer effects, and flowback production, and combine numerical simulations with artificial intelligence algorithms to infer fracture network parameters, although the issue of non-uniqueness in solutions remains to be addressed. Research shows that no single technology can comprehensively characterize fracture network features. Future directions should involve the integration of multi-source data (geophysical, chemical, fiber-optic, and dynamic production data) to construct intelligent evaluation frameworks, validated by field experiments and dynamic data simulations. The introduction of artificial intelligence and big data technologies provides new ideas for fracture network parameter inversion, but their effectiveness still requires support from more case studies. This paper provides theoretical guidance and practical reference for the optimization and integration of fracture network evaluation technologies in efficient shale gas development.

Keywords: shale gas development; hydraulic fracture characterization; direct monitoring techniques; dynamic parameter inversion

check for updates

Academic Editor: Tiago Filipe da Silva Miranda

Received: 8 July 2025
Revised: 3 August 2025
Accepted: 8 August 2025
Published: 15 August 2025

Citation: Yuan, H.; Sun, Y.; Xiong, W.; Niu, W.; Tang, Z.; Li, Y. Advances in Evaluation Methods for Artificial Fracture Networks in Shale Gas Horizontal Wells. *Appl. Sci.* **2025**, *15*, 9008. https://doi.org/10.3390/app15169008

Copyright: © 2025 by the authors. Licensee MDPI, Basel, Switzerland. This article is an open access article distributed under the terms and conditions of the Creative Commons Attribution (CC BY) license (https://creativecommons.org/licenses/by/4.0/).

1. Introduction

Over the past decade, with breakthrough advancements in horizontal drilling and hydraulic fracturing technologies, the development of unconventional oil and gas resources—represented by shale gas—has entered a golden era [1]. Compared to conventional reservoirs, the matrix permeability of shale gas formations is typically below 1000 nD (10^{-9} μm^2), exhibiting nanoscale pore flow characteristics [2]. As a result, complex artificial fracture networks must be created through multi-stage fracturing in horizontal wells to significantly increase the contact area between the fracture network and the shale matrix, thereby enabling large-scale and effective shale gas production. However, the morphology

of fracture networks is controlled by the nonlinear coupling of multiple factors, including rock brittleness index, in situ stress anisotropy, the degree of natural fracture development, and fracturing operation parameters [3].

At present, a systematic understanding is still lacking regarding fracture propagation criteria, mechanisms of competing growth among multiple fractures, and the spatial topology of fracture networks [4,5]. This deficiency in mechanistic understanding directly hampers the establishment of a quantitative mapping relationship between geological-engineering parameters and fracture network stimulation outcomes in engineering practice. Consequently, this limits the precise implementation of "sweet spot" targeted fracturing and fracture network control technologies [6].

Currently, the evaluation system for fracture network stimulation effects in shale gas reservoirs mainly focuses on two dimensions: geometric characterization and flow efficiency. Geometric characterization includes morphological parameters such as fracture length, height, stimulated volume, and branching complexity, while flow efficiency involves dynamic indices such as proppant transport and distribution, temporal-spatial evolution of conductivity, and two-phase gas–water flow characteristics [7]. Existing evaluation methods can be broadly categorized into two technical routes: direct monitoring and dynamic inversion [8]. The former obtains physical parameters of the fracture network through geophysical and chemical tracer methods, whereas the latter infers them using fracturing treatment curves, flowback, and production data.

This paper systematically reviews recent advancements in direct monitoring technologies such as microseismic monitoring, tracer tracking, wide-field electromagnetic methods, and distributed fiber optics. It also analyzes the current state of dynamic inversion methods from perspectives such as transient fracturing response, shut-in water hammer effect, flowback dynamic analysis, and production capacity simulation. Finally, the paper proposes an intelligent evaluation framework based on multi-source data fusion as a future direction. This work provides theoretical foundations and practical reference for optimizing and integrating fracture network evaluation technologies in efficient shale gas development.

2. Direct Monitoring

Current direct monitoring techniques for shale gas fracture networks are primarily based on three physical principles:

1. Geophysical Field Responses: By capturing field signals induced by hydraulic fracturing, such as seismic waves (microseismic monitoring) and electromagnetic anomalies (wide-field electromagnetic methods), the spatial distribution of fractures can be inferred;
2. Chemical Tracer Migration: The transport behavior of radioactive or non-radioactive tracers within the fracture network is utilized to analyze fracture connectivity and proppant distribution;
3. Fiber-Optic Sensing Responses: Distributed fiber-optic systems detect disturbances in temperature or acoustic signals to enable in situ monitoring of fracture initiation, propagation, and closure.

Due to differences in physical principles, each technology varies in terms of resolution (ranging from meter- to centimeter-scale), monitoring scale (from near-wellbore regions to block-level coverage), and temporal responsiveness (from real-time to delays of several days). This section focuses on analyzing the physical mechanisms, field application challenges, and recent advancements of mainstream direct monitoring techniques.

2.1. Microseismic Monitoring

Microseismic monitoring, a geophysical remote sensing technique, enables real-time or post-acquisition detection and spatial imaging of fracture activity by continuously recording microseismic signals induced by hydraulic fracturing via three-component geophone arrays deployed in observation wells or at the surface [9]. The underlying physical mechanism is that hydraulic fracturing in shale formations alters local pore pressure and in situ stresses, leading to brittle failure (tensile fracturing) of intact rock or shear slip along natural fractures [10]. Approximately 0.1–1% of the elastic wave energy released from these rupture processes propagates to the surface as microseismic waves. Through spectral analysis, traditional machine learning, and deep learning algorithms, microseismic events can be effectively identified and located [11], producing volumetric maps that represent the extent of shear and tensile fracturing in the rock mass [12].

As the only available technique capable of providing real-time three-dimensional information on fracture network evolution, microseismic monitoring allows reconstruction of fracture network geometry (length, height, azimuth) by inverting event locations, facilitates quantitative calculation of Stimulated Reservoir Volume (SRV), and provides feedback to optimize fracturing parameters such as injection rate and proppant concentration [13]. According to the Society of Petroleum Engineers (SPE), over 90% of hydraulic fracturing operations in shale gas horizontal wells worldwide have adopted this technique for process monitoring [14].

Microseismic monitoring is categorized into surface-based and downhole-based systems (Figure 1) [15]:

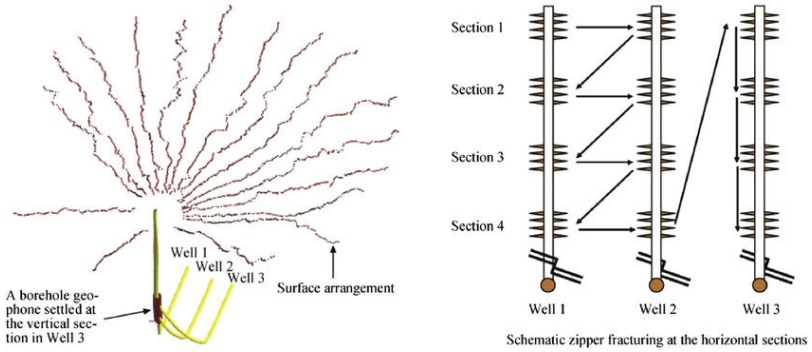


Figure 1. Schematic Diagram of Surface and Borehole Microseismic Monitoring Systems [16].

Surface monitoring systems typically consist of 500–2000 surface geophones arranged in a regular grid with spacing ranging from 100 to 500 m. The array density can be flexibly adjusted to meet different monitoring needs: single-well monitoring commonly uses a 1 km × 1 km grid, multi-well pad operations expand coverage to 3 km × 3 km, and regional monitoring can reach up to 10 km × 10 km [17]. This topological flexibility enables the acquisition of critical parameters such as fracture azimuth (±5° error) and fracture length (±10% error), providing direct guidance for well placement and spacing. Surface monitoring relies solely on P-waves (compressional waves) for event location, avoiding the complications of S-wave (shear wave) usage [18]. Since S-wave velocity models are more sensitive to formation anisotropy and fracture filling materials, they often lead to increased uncertainty, whereas P-wave models remain relatively stable even when simplified, maintaining acceptable accuracy [19].

With surface microseismic monitoring, the wave propagation path from underground fractures to the surface is typically long and nearly vertical, causing localized velocity anomalies (e.g., small-scale fractures, rock heterogeneity) to be averaged out. This reduces the sensitivity of event locations to lateral velocity variations, making surface monitoring

well-suited for long-term tracking of pressure and stress changes during production [20]. However, three major technical bottlenecks remain:

1. The cost of large-scale array deployment increases exponentially. A 3000-channel geophone system can exceed USD 2 million;
2. Simplified P-wave velocity models limit vertical resolution (tons of meters);
3. Industrial noise sources (e.g., pumping units >90 dB, rig vibrations 10–50 Hz) overlap with the microseismic frequency band (100–1000 Hz), requiring advanced adaptive filtering and deep learning denoising algorithms to improve signal-to-noise ratio [21].

Downhole monitoring adopts a "wellbore-to-surface" hybrid observation mode, where 12–24 levels of three-component geophones are deployed in nearby offset wells and integrated with surface arrays to form a 3D observation network. This setup combines cost efficiency with high resolution, particularly effective for controlling fracture height (e.g., avoiding caprock breach). However, due to constraints of the wellbore, horizontal location errors can reach 20–50 m, and applicability is limited by the availability of observation wells [22].

Over the past 40 years, microseismic monitoring has undergone three major stages of technological evolution. Its global application coverage in shale gas plays now exceeds 92%, making it the "gold standard" for hydraulic fracturing monitoring [23,24]. Nevertheless, the technique still faces several limitations:

1. Lack of standardized magnitude calibration [25]: Accurate magnitude estimation is crucial for calculating stimulated rock volume and guiding fracturing operations [26]. However, traditional magnitude formulas were developed for larger-scale seismic events, leading to discrepancies in event magnitudes when extrapolated to microseismic scales;
2. High-frequency signal attenuation at depth: In deep shale formations (>3500 m) such as those in the Sichuan Basin, more than 70% of microseismic events cannot be detected by surface arrays due to severe signal attenuation [27];
3. Uncertainty in fracture parameter inversion: Microseismic monitoring essentially captures acoustic emissions, identifying rupture points rather than full fracture geometries. Parameters like fracture length and conductivity are influenced by monitoring geometry and inversion models, requiring integration with geomechanical simulations and facing issues of non-uniqueness [28].

2.2. Tracer Monitoring

Tracer monitoring involves injecting substances with unique chemical or physical signatures (such as rare earth elements or radioactive isotopes) and interpreting the concentration changes in flowback fluids to infer characteristics of the fracture system (Figure 2). This technique can be used to evaluate [29]:

- Spatial distribution of proppant;
- Supplementary fracture characterization;
- Contribution of individual fracturing stages;
- Inter-well interference intensity.

New generations of tracers are becoming increasingly functionalized [30–32]: near-well monitoring typically utilizes gadolinium-tagged proppants, while mid- and far-field detection can employ tracers with electromagnetic responses [33].

Conventional chemical tracers must meet dual stability requirements—physical and chemical—to ensure synchronized transport in both gas and water phases. The main types of tracers used in fracture evaluation include [34]:

1. Emulsified Tracers: Composed of water/oil dual-phase soluble tracers, they are co-injected with the fracturing fluid through an emulsification process. Their phase-selective solubility enables multi-phase flow dynamic monitoring within the matrix-fracture system.
2. Perforation Tracers: Made of high-temperature-resistant metal-based composite tracer materials (e.g., tungsten-rare earth oxides), which are embedded into the cemented multi-stage fracturing system using perforation charge integration. These tracers are released upon activation by high temperatures (>800 °C) during the perforation phase, and are mainly applied in cement plug and perforation fracturing operations.
3. Controlled-Release Tracers: Polymer-based tracer compounds placed on the exterior of production casing that gradually release tracers upon contact with formation fluids.

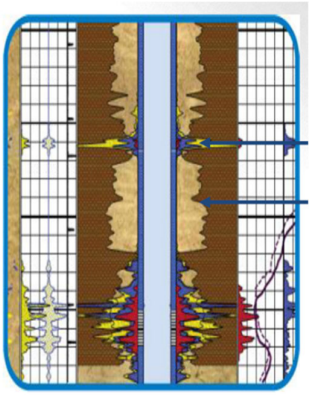


Figure 2. Monitoring Fracture Height Extension.

In field development, tracers are typically categorized into five types [35]: Dye tracers, Radioactive tracers, Water-soluble alcohol tracers, Cationic/anionic tracers, Gaseous tracers.

Due to variations in geological conditions, it is rarely possible to identify a "perfect" tracer that satisfies all operational criteria. Nonetheless, tracer selection should adhere to the following principles:

- Solubility and co-migration with the carrier fluid at matching velocities;
- Chemical stability (excluding radioactive tracers) without adsorption or degradation;
- Low natural background concentration in the target formation for high signal-to-noise detection;
- Detectable in trace quantities with high-sensitivity analytical methods;
- Cost-effectiveness, considering synthesis, injection, and detection costs;
- Safety and environmental compliance throughout injection and production stages;

Analytical methods for tracer monitoring generally fall into three categories [36]: Qualitative analysis, Analytical (semi-analytical) modeling and Numerical modeling.

2.2.1. Qualitative Analysis

Qualitative analysis is the most widely used approach in tracer monitoring. It is commonly applied for preliminary assessments of reservoir connectivity, analysis of inter-well communication patterns, identification of high-permeability flow paths, and recognition of flow barriers [37,38]. For example, Kuma et al. analyzed combined tracer and pressure interference tests and observed that zipper-fractured wells had higher tracer recovery rates, indicating better fracture network connectivity. Early tracer signals showing interlayer communication later disappeared during production, suggesting the closure of unpropped fractures [39]; Li et al. developed three types of delayed-release tracers to quantitatively determine stage-specific contributions in horizontal wells. By comparing peak tracer arrival times and annular volume differentials, they successfully calculated segmental contribu-

tions. The results aligned well with numerical simulations [40]; Katashov et al. applied chemical tracers coated on proppant surfaces, injecting uniquely coded tracer-proppant combinations in each fracturing stage. They developed a tracer-based production logging technique that does not require well shut-in or downhole intervention, making it suitable for long-term monitoring. This enabled optimization of stage count, proppant loading, and fracture geometry to enhance recovery [41]; Roshan et al. proposed a novel technique based on cation exchange and chemical tracers. During fracturing, high-concentration cations (e.g., Na^+) are injected to displace native cations (e.g., Ca^{2+}, K^+) on shale clay mineral surfaces. The concentration of released cations correlates with fracture surface area, offering a method to characterize fracture area and optimize fracturing design [42]; In California's Antelope Shale (Monterey Formation), oil-phase chemical tracers were used to assess vertical production contributions across different intervals. The technology successfully identified high-yield zones and, by providing long-term dynamic data, reflected the true productive potential of the reservoir [43].

2.2.2. Analytical (Semi-Analytical) Modeling

As early as 1965, Brigham et al. proposed a semi-analytical model that derived a mixing equation under radial flow conditions, incorporating dispersion coefficients and pore volume to predict tracer concentration distributions [44]. The model was validated through a five-spot well pattern field test, analyzing how permeability layering influences tracer breakthrough curves. In 1984, Brigham and colleagues extended the original model by introducing the concept of stream tubes in multilayer systems. This advancement enabled analytical solutions to account for vertical dispersion. By inverting tracer curves, the model could estimate the porosity thickness and permeability thickness of products across layers, effectively characterizing reservoir stratification [45]. Jeasen developed a dual-porosity model that included adsorption, matrix retention effects, and nonlinear variations in physical properties. The results confirmed that diffusion and adsorption are primary mechanisms of tracer retention. Neglecting matrix diffusion would overestimate fracture velocity and underestimate fracture width, although the model did not incorporate in-fracture fluid dispersion, potentially affecting late-time data fitting [46]. Rivera conceptualized the reservoir as alternating zones of equally spaced, parallel fractures and porous matrix blocks, categorized as follows.

Fracture zones: dominated by convection and diffusion, Matrix zones: governed solely by diffusion and linear adsorption; these two zones are connected via stagnant fluid films. The newly proposed model reduced the number of fitting parameters, enhancing computational efficiency [47]. Tian introduced a zonal chemical tracer model that estimates fracture volume and fluid loss volume based on injection and production data [48]. The study found that high distribution coefficients (K-values) led to rapid flowback but only reflected the near-well swept volume, underestimating actual fracture volume; in contrast, low-K tracers penetrated deeper but returned more slowly and could overestimate fracture volume. Kumar et al. developed a coupled model integrating geomechanics, fluid flow, and tracer transport to simulate fracture propagation, closure, tracer injection, and recovery. Their findings showed that multi-peaked tracer curves could result from fracture closure, while low recovery rates were attributed to both fracture closure and initially low water saturation in the reservoir. They introduced the concept of "effective connected fracture length," which, when combined with tracer data, can optimize fracturing design and production forecasting [49].

2.2.3. Numerical Modeling

With advances in computational technology, mathematical modeling and simulation of tracer test results have become a new research focus. In 1993, Holditch et al. used 3D geological modeling to predict fracture height and width, and the simulation results qualitatively matched tracer observations [50]. Lange et al. employed a Discrete Fracture Network (DFN) model, integrating tracer test and production data, to numerically estimate fracture half-length and conductivity. Joint inversion of tracer and production data effectively constrained both parameters and validated the reliability of the DFN model [51]. Ghods et al. [52] proposed a partitioned dual-porosity model combined with the Ensemble Kalman Filter (EnKF) to automatically estimate fracture attributes. This model reduced the required input parameters, needing only production and tracer data. Elahid et al. [53] applied the EnKF method to jointly invert fracture half-length and conductivity using tracer test and production data. They found that tracer data effectively constrained fracture conductivity, while production data were more suitable for estimating fracture half-length. The integration of both datasets allowed simultaneous optimization of both parameters. In a follow-up study, Elahid compared two models (planar fracture vs. DFN), each tested with only tracer data or only production data. Results showed that in the DFN model, tracer data were more sensitive to fracture conductivity and density, while production data were more sensitive to fracture density and matrix permeability [54]. Liu et al. considered tracer dispersion and adsorption mechanisms, and developed a high-efficiency numerical model based on the Embedded Discrete Fracture Model (EDFM). This model was designed to characterize complex fracture networks and simulate tracer flowback behavior. Sensitivity analysis showed that fracture conductivity and adsorption effects significantly influenced tracer return characteristics [55].

Tracer monitoring is considered one of the most cost-effective diagnostic techniques and has, over time, developed a solid theoretical foundation. It is relatively easy to implement and interpret. However, several limitations still exist in practical applications [56]:

1. Radiotracer attenuation: Radioactive tracers experience significant attenuation when passing through casing, cement sheaths, and surrounding rock. Additionally, isotopes with short half-lives are often unsuitable for long-term monitoring (e.g., >30 days after fracturing) [57].
2. Limited resolution in far-field fracture detection: Due to the constraints of tracer diffusion coefficients, current techniques primarily characterize proppant distribution near the wellbore.
3. Detection resolution for far-field fracture extension remains insufficient [58]. Stability under harsh conditions: High-temperature or high-salinity environments may compromise tracer chemical stability, reducing monitoring reliability [59].
4. Limited spatial resolution and diagnostic independence: Tracer data often lack the resolution required to map fine-scale fracture geometries. As such, their diagnostic capabilities should be viewed as complementary, rather than standalone.

2.3. Wide-Field Electromagnetic Monitoring (WFEM)

The Wide-Field Electromagnetic Method (WFEM) was first proposed by He et al. in 2010 as a theoretical framework [60]. Its core innovation lies in constructing analytical solutions for the coupled electromagnetic fields generated by horizontal electric dipoles and vertical magnetic dipoles in a semi-infinite medium (Figure 3) [60]. By applying adaptive finite element algorithms, global apparent resistivity inversion is achieved, overcoming the distance limitations of traditional electromagnetic techniques [61]. Compared to Conventional Controlled-Source Audio Magnetotellurics (CSAMT), WFEM offers three

major technical advantages [62]: Strong noise resistance, Deep detection capability, High-efficiency data acquisition.

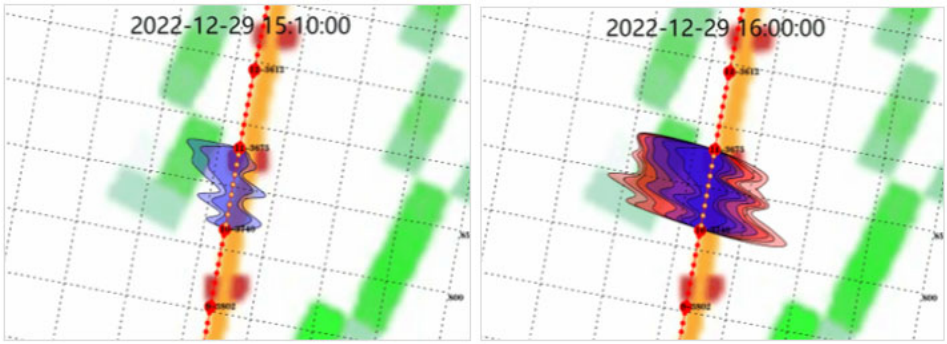


Figure 3. Monitoring Hydraulic Fracture Growth Using Wide-Field Electromagnetic Method.

Initially developed for applications in mineral exploration, geothermal resources, deep brine lakes, and hydrocarbon prospecting [63], WFEM has since been adapted to shale gas reservoirs. Yuan et al. compared the applicability of logging, seismic, and WFEM techniques under complex geological conditions in southern China. In the Chongkou Block, WFEM performed reliably in rugged terrain, successfully identifying shale gas reservoir distributions and fault zones. Combined with logging data, it helped locate "sweet spots" with high gas content, providing crucial guidance for exploration [64]. Yang et al. [65] applied WFEM in the Huayuan Block, Hunan Province, to identify geological structures, target layer distributions, and thickness. Based on associated logging parameters, high-potential shale gas zones were screened. WFEM proved well-suited for complex terrain in southern China, enabling effective identification of target layers, thicknesses, and faults. Through correlations with resistivity, induced polarization (IP), and TOC content, high-potential zones could be selected, thereby reducing exploration risk. In 2020, Xie et al. [66] proposed an interpolation method based on random forest regression to address data loss and noise issues caused by equipment limitations and human interference during WFEM. This provided a novel data-processing approach for hydraulic fracturing diagnostics. Yang et al. used WFEM instruments to establish a harmonic electromagnetic field through artificial grounding sources, observed field components, and calculated wide-field apparent resistivity for subsurface fracture detection [67]. This method was effective in analyzing natural fractures, diversion effects from temporary plugging, and interstage interference—thus improving stimulation efficiency and well productivity. The monitoring outcomes provided optimization references for deep shale hydraulic fracturing in horizontal wells. Ye et al. [68] applied WFEM during a temporary plugging operation in southern Sichuan, achieving 10 min update intervals. The system dynamically visualized fracture geometry, affected area, and fracture length, supporting real-time adjustment of fracturing parameters. Monitoring results corroborated geological predictions, showing that fluids more readily extended along low-stress paths near faults and natural fracture zones. Hu et al. [69] collected WFEM data from a shale gas well in Guizhou Province, using three monitoring rounds—before, during, and after fracturing—for differential analysis. Fracture extension direction and geometry were identified. Constrained by drilling data, precise inversion revealed fracture height and length. This demonstrated that WFEM, through differential analysis and deep inversion, can quantitatively evaluate fracturing effectiveness. Tie et al. [70] used WFEM to monitor fracturing in the DX185 Block, confirming in real time the extent of fracturing fluid coverage and fracture network morphology. The technique proved suitable for complex geological conditions in Xinjiang.

Despite its advantages, the WFEM technique currently faces three major bottlenecks [71]:

1. Economic Constraints: The cost of a single 3D monitoring campaign is significantly high—approximately 2 to 3 times that of microseismic monitoring. This limits its widespread deployment in commercial field operations.
2. Inversion Non-Uniqueness: Different inversion algorithms (e.g., Occam or Marquardt) can yield resistivity results with 15–25% variability, leading to fracture length estimation deviations of up to ±20%. The inherent ill-posed nature of electromagnetic inversion makes it sensitive to initial conditions and algorithm selection.
3. Geological Adaptability: In areas with low-resistivity overburden, the attenuation rate can reach 0.8 dB/m, which severely reduces detection resolution for deep fractures (>3 km)—vertical resolution can decline to ±50–100 m at such depths.
4. Environmental Electromagnetic Interference: During field acquisition, WFEM is highly susceptible to electromagnetic interference from surface infrastructure, such as power lines, metal pipelines, and other electromagnetic noise sources. These interferences degrade data quality and increase inversion instability. Special precautions must be taken during deployment in such environments.

2.4. Distributed Fiber-Optic Monitoring (DTS, DAS)

Since its commercialization in the 1990s, distributed fiber-optic sensing technology has gradually become a core technique for dynamic monitoring in oil and gas reservoirs. The first industrial application occurred in 1996 in the Coalinga Oilfield (USA) during steam injection monitoring [72]. In 2006, distributed temperature sensing (DTS) was first used in a 230 m deep vertical well in Indonesia to monitor real-time fracture height during microfracturing treatments [73]. In hydraulic fracturing operations, the two most commonly used fiber-optic technologies are: DTS (Distributed Temperature Sensing), DAS (Distributed Acoustic Sensing). These systems operate by detecting variations in the backscattered light along the optical fiber, which reflects changes in temperature and acoustic fields [74]. The primary scattering mechanisms include: Rayleigh scattering, Brillouin scattering, Raman scattering [75].

In Raman scattering, anti-Stokes components (those with frequencies higher than the incident light) are particularly sensitive to temperature changes—their intensity increases significantly with temperature [76]. During hydraulic fracturing, temperature profiles along horizontal wellbores often exhibit characteristic sawtooth-like oscillations (Figure 4). Major fractures correspond to regions of sharp temperature drops; the lower the temperature, the longer the fracture. By inverting the real-time temperature field, asymmetric fracture propagation can be evaluated online [77]. By analyzing the distributed temperature field along the fiber, a comprehensive picture of fracture distribution can be obtained [78]. Temperature-induced changes in optical signals are converted into electrical signals, enabling physical field temperature measurement [79].

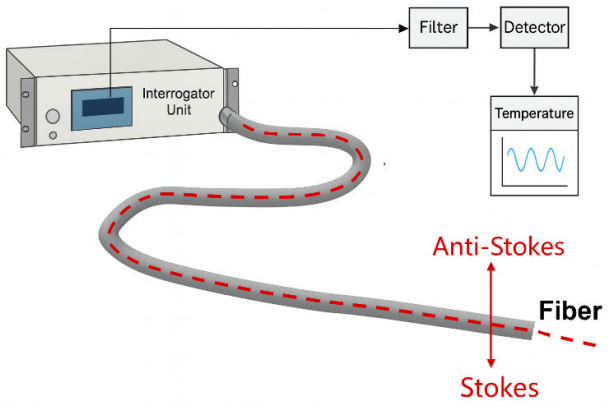


Figure 4. Schematic Diagram of DTS Working Principle.

DTS-based fracture diagnostics mainly follow two modeling approaches: Numerical modeling of fluid expansion, conduction, and convective heat transfer near the wellbore–fracture interface, considering viscous dissipation and temperature variations; and Post-fracturing flowback analysis, using temperature data to assess fracture effectiveness [80]. Tarrahi coupled mass and energy conservation equations, initially assuming a uniform fracture half-length. By comparing simulated and actual DTS data, parameters were updated using a Kalman gain matrix [81]. The EnKF method efficiently inverted fracture parameters. However, DTS data showed high sensitivity to fracture count and reservoir permeability, but limited sensitivity to fracture conductivity. Yoshida et al. developed a temperature prediction model that couples the wellbore and reservoir using mass conservation, Darcy's law, and transient energy balance (including conduction, convection, viscous dissipation, and fluid expansion) [82]. After production stabilizes, the temperature profile can be inverted to determine fracture geometry, helping evaluate conductivity in real time. Kalia et al. [83] used mass, momentum, and energy conservation laws, accounting for fluid loss to the formation, to calculate pressure, velocity, and temperature distributions in the wellbore. By minimizing the difference between simulated and measured DTS temperatures, reservoir permeability and fracture flow rates were iteratively adjusted. Cui developed a semi-analytical fracture model dividing the reservoir into fracture, inner high-permeability zone, and outer original-permeability zone. The model incorporated convective and conductive heat transfer, as well as Joule–Thomson effects caused by pressure drops, using temperature changes to identify fracture locations [84]. Sun et al. [85] coupled a non-isothermal reservoir model with an EOS-based IMPEC (Implicit Pressure, Explicit Composition) component model. The reservoir simulation accounted for multiphase flow, heat conduction, and convection. The wellbore model used finite difference methods and drift-flux or two-fluid flow models, solving mass, momentum, and energy equations with Joule–Thomson effects, and performed sensitivity analysis on fracture parameters. Results showed that central fractures exhibited the lowest temperatures, while edge fractures—due to more favorable heat exchange—were warmer. Significant temperature asymmetry was observed due to variations in fracture conductivity.

The working principle of Distributed Acoustic Sensing (DAS) (Figure 5) is based on the phase and intensity variations in Rayleigh backscattered light along the optical fiber [86]. In 2009, Shell conducted the first field application of DAS in a tight gas well in Canada. Jin proposed monitoring strain and temperature variations during fracturing using low-frequency DAS signals (<0.05 Hz) to constrain fracture geometry parameters [87]. DAS signals can identify fracture initiation (highlighted as red extension zones), closure (blue compression zones), and stress shadows (compressed zones adjacent to active fractures). Fracture length is determined by comparing the signal coverage range with the designed stage length, enabling real-time monitoring of fracture propagation. Sherman introduced a hybrid method combining physical modeling and deep learning, using DAS to monitor subsurface hydraulic fracturing. The input data included pre-processed DAS signals and the distance between the fiber and the fractures. The algorithm output labeled fracture parameters such as height and location [88]. Titov analyzed DAS Vertical Seismic Profiling (VSP) data to study scattering behaviors, dynamically monitoring changes in Stimulated Reservoir Volume (SRV), fracture closure timing, inter-well interactions, and SRV geometry (height and length), offering important insights for fracturing optimization [89]. Li et al. used single-well fiber-optic monitoring to evaluate fracturing effectiveness in three offset wells and the fiber-optic well. In Well A, DAS/DTS data revealed uneven cluster efficiency, with some clusters receiving significantly less proppant than the designed 25%. DAS signals from Well A also detected fractures from nearby Wells B, C, and D. On average,

Well B showed 7.1 fractures per stage, while Wells C and D detected only 3.2 fractures per stage [90].

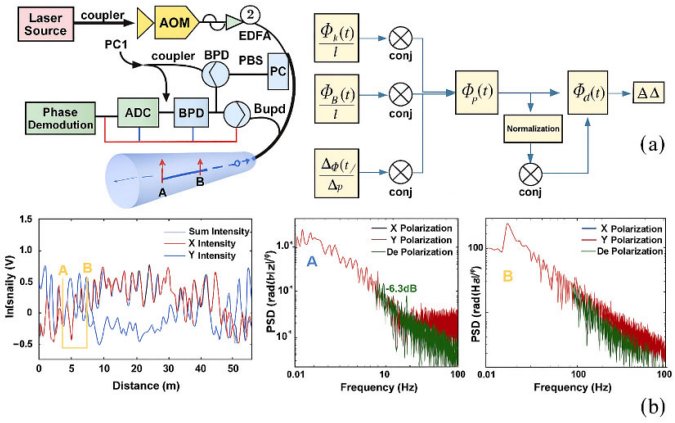


Figure 5. Polarization-Demodulated DAS System Architecture and Signal Processing Workflow (**a**) The experimental setup. (**b**) The chirped pulse and its division into sub-bands (offset for better visibility; the frequency change is linear across the entire range) [91].

Although distributed fiber-optic sensing can evaluate multiple geometric and flow characteristics of artificial fracture networks, it still faces the following limitations [92]:

1. High cost of sensors and deployment: the installation and maintenance of distributed optical fibers are capital-intensive. Specialized hardware, fiber-optic cables, and permanent downhole installations drive up overall operational costs.
2. Massive data generation and management challenges: continuous monitoring produces vast quantities of data. Challenges arise in data storage, processing, visualization, and security, especially in large-scale multi-well applications [93].
3. Risk of fiber damage during fracturing operations: the high-pressure injection of fracturing fluids and proppants may damage optical fibers—especially when placed inside the wellbore—compromising long-term data acquisition.
4. Immature data interpretation models and tools: current software platforms and theoretical models for interpreting DTS/DAS signals are still under development. Effective analysis requires interdisciplinary knowledge of optics, mechanics, geophysics, well logging, and hydraulic fracturing [94].

2.5. Field Experiments and Core Analysis

Field-scale experiments offer a unique advantage by enabling direct, in situ studies of specific hydraulic fracturing processes. The real-time monitoring data obtained from such experiments can provide robust guidance for engineering practices. In 2015, the U.S. Department of Energy (DOE) launched the Hydraulic Fracturing Test Site (HFTS) program, which integrates resources from the National Energy Technology Laboratory (NETL), international energy corporations (e.g., Shell, Chevron), and academic institutions (e.g., The University of Texas at Austin) to establish a three-pronged research paradigm of field-scale fracturing–core analysis–laboratory characterization.

The project led to the creation of the world's first public shale fracturing database and systematically investigated fracture propagation dynamics, proppant transport mechanisms, and fluid efficiency optimization strategies. These efforts have significantly reduced groundwater contamination risks and accelerated the standardization of fracturing technologies. Two experimental phases have been successfully implemented to date [95].

The first-phase experiment was conducted in the Wolfcamp Formation of the Midland Basin, Reagan County, Texas, focusing on the Upper and Middle Wolfcamp intervals. A 3D

observation network was established, including production wells, monitoring wells, and deviated coring wells [96,97]. A key innovation was the angled trajectory of the coring well, designed to intersect the primary stimulated zone. This approach successfully retrieved continuous core samples [98]. Trajectory design was optimized based on microseismic results, ensuring the cores would intersect the dominant fracture orientation aligned with the maximum horizontal stress (SHmax) [99]. Gale et al. directly observed hydraulic fractures in cores extracted from deviated wells to analyze fracture types, distribution, and reactivation of natural fractures [100]. Multiple bifurcated fractures and surface markings (e.g., hackles) were observed, indicating fracture orientations. Most hydraulic fractures trended east–west, consistent with regional SHmax. Some natural fractures were reactivated, but most remained sealed. Maity et al. analyzed the distribution of proppants and natural calcite grains in core and cuttings samples to understand proppant transport behavior within the Stimulated Reservoir Volume (SRV) and its interactions with perforation clusters and natural fractures [101]. Proppant clusters correlated with carbonate layer boundaries, lithological changes, or stress gradients. Notably, microseismic event coverage (~500 ft vertical) far exceeded the actual proppant penetration (~25 ft), indicating limited conductivity. In zones with dense natural fractures, proppant concentration was low, possibly due to complexity-induced trapping. The transport behavior of proppants showed clear patterns: finer particles (e.g., 100 mesh) tended to migrate further laterally, while localized proppant accumulation often occurred near stress contrasts or layer boundaries, where fractures bifurcated. Li evaluated the fracture systems in the Wolfcamp A and Wolfcamp B formations using Rate Transient Analysis (RTA), Pressure Interference Testing (PIT), and reservoir pressure depletion analysis [102]. Results showed that fracture closure in Wolfcamp A occurred faster than in B. Deviated well data revealed higher fracture conductivity near the wellbore. Wolfcamp A responded more favorably to high proppant loading, whereas Wolfcamp B would require design optimization to improve stimulation effectiveness. Maity employed high-resolution 3D laser scanning technology to generate digital surface maps of fracture faces on core samples. By removing scanning artifacts and using Principal Component Analysis (PCA) to reorient the fracture planes, the researchers fitted flat surfaces to calculate roughness metrics. Results indicated that fracture roughness strongly correlated with localized proppant trapping; in rough zones (e.g., in the Upper Wolfcamp, UWC), localized proppant bridging was more likely to occur, forming thick proppant beds [103]. Additionally, fracture orientation was found to exhibit a power–law relationship with roughness. Salahshoor et al. analyzed over 400 fracturing stages across 11 horizontal wells in the HFTS project. They found that in certain intervals, fracture gradients were predominantly governed by formation properties (e.g., permeability, vertical stress, pore pressure), while in others, the gradients were more dependent on completion parameters, such as proppant size ratio and perforation density [104]. In a related study, Salahshoor also noted that increasing perforation density in clay-rich zones led to decreased production, while in brittle formations, higher perforation density improved productivity [105]. Male statistically analyzed 600 feet of inclined core (containing 375 hydraulic fractures) using Bayesian methods to assess the relationship between fracture density and reservoir properties. Hydraulic fracture density decreased with vertical distance from the fractured well, with the most significant drop in carbonate layers. In areas of high natural fracture density, fewer hydraulic fractures were observed—even when controlling for lithology—suggesting stress interference or fracture competition as influencing factors.

Building on the discoveries of the first HFTS experiment—particularly regarding hydraulic fracture geometry and proppant distribution—Laredo Petroleum and GTI, with funding from the U.S. Department of Energy and industry sponsors, launched the second-phase experiment (HFTS-2) in the Delaware Basin, Block 55, near Loving County,

Texas [106]. HFTS-2 involved eight new production wells and two existing parent wells, where hydraulic fracturing treatments were conducted. A vertical pilot hole was drilled to collect 540 feet of core along with 950 feet of high-angle core that intersected hydraulic fractures [107]. Gale identified a total of 1261 fractures in the 948-foot-long deviated core, among which 500 were confirmed as hydraulic fractures. These hydraulic fractures often appeared in clusters, with some clusters containing up to five fractures, and commonly exhibited step-like or feathered structures [108]. Zhang et al. integrated fiber-optic, microseismic, and other diagnostic data to reveal fracture propagation behaviors during HFTS-2 [109]. Key findings included: (1) Asymmetric growth—DAS low-frequency data showed that fractures extended more vertically upward than downward. (2) Stratification effects—Vertical heterogeneity in lithology led to layered fracture development, whereas in homogeneous intervals, fractures were more elliptical in shape. Bessa combined data from geology, petrophysics, geochemistry, geomechanics, microseismic, fiber-optic sensing (FO), and bottomhole pressure gauges (BHPG) to characterize the hydraulic fracture networks at HFTS-2. Among the 500 identified hydraulic fractures, most were planar, with some exhibiting stepped or feathered morphologies. The concentration of proppants in flowback fluids correlated with activated fracture density, offering insight into fracture effectiveness [110]. Pudugramam analyzed an integrated dataset from HFTS-2 to: quantify the vertical and lateral extent of hydraulic fractures; and assess the effect of parent well depletion on child well fracture geometry.

Results showed that in overlapping regions with depleted parent wells (southern section), child well fractures extended more toward the east, but had shorter half-lengths and reduced heights compared to those in non-depleted zones (northern section). Significant surface pressure responses in parent wells during child well stimulation confirmed fracture communication between wells [111].

Field-scale experiments currently provide the clearest and most direct understanding of reservoir behavior. They form a solid foundation for subsequent efforts in geological modeling [112] and production simulation [113], and offer valuable platforms for advancing fundamental theory and validating monitoring technologies.

However, due to their high cost and resource-intensive nature, such detailed experimental analyses cannot be performed on every well. Additionally, the findings from the HFTS program are most applicable to the Wolfcamp and Delaware Basin formations, where the experiments were conducted. In geologically different regions, the direct applicability of these conclusions may be limited.

3. Dynamic Inversion

Based on the full life-cycle stages of shale gas development, the dynamic inversion system can be deconstructed into four temporal modules (Figure 6): fracturing stage, shut-in stage, flowback stage, and stable production stage.

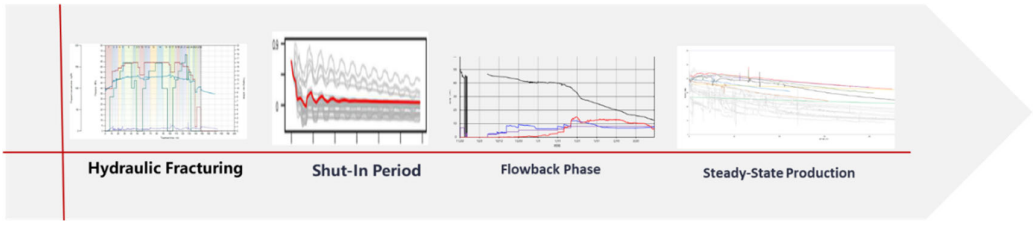


Figure 6. Development Phases and Corresponding Dynamic Data in Shale Gas Operations.

Each stage exhibits distinct data characteristics. The fracturing and shut-in stages primarily rely on high-frequency pump-in data (on the order of seconds) to achieve real-

time fracture diagnostics. In contrast, the flowback and production stages focus on dynamic, multiphase flow data (gas and water) to infer the spatial-temporal evolution of fracture network conductivity.

3.1. Fracture Evaluation Based on Fracturing Stage Treatment Curves

Fracturing treatment curves contain rich information regarding the evolution of the fracture network (Figure 7). Key parameters include treatment pressure, injection rate, proppant concentration, and fluid volume. In 1981, Nolte pioneered the use of pressure diagnostics by introducing a log–log plot slope criterion. By plotting net pressure versus log (time), different slopes could be used to infer distinct fracture propagation modes [114]. Specifically, a slope of $0.14 < e < 0.25$ indicates stable fracture growth with height containment. A flattening trend suggests fracture extension has reached a stress barrier (e.g., entering a high-stress layer, activation of secondary fractures, or increased fluid loss due to screenout). A slope of 1 indicates rapid height growth or increased fluid loss, while a negative slope suggests accelerated fracture height extension.

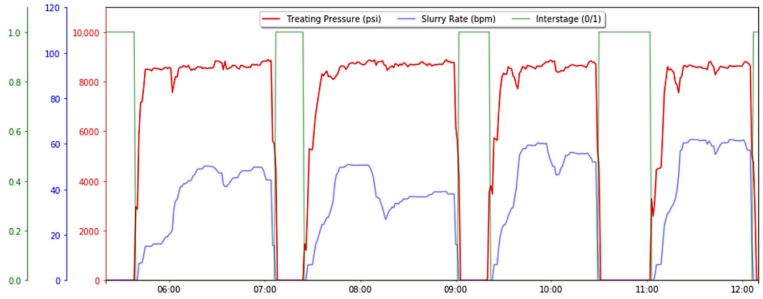


Figure 7. Example of Fracturing Pump-In Data.

This method is based on several core assumptions [115]: the formation behaves as a quasi-elastic medium, with no interlayer slip

A power–law fluid is continuously injected

After shut-in, fractures stop propagating, and closure is not significantly affected by the proppant. Subsequent researchers have extended and refined this model.

In 2013, Pirayesh improved upon the Nolte-Smith theory by implementing dynamic reference point adjustments (instead of fixed initial time points) and incorporating power–law fracture growth models with numerical algorithms for real-time diagnostics. Compared to traditional Nolte–Smith methods, the new model—known as Moving Reference Point (MRP)—allowed for faster recognition of fracture behavior and did not require closure stress input [116]. Al-Husain applied the MRP method to real-time fracture diagnostics in the Cotton Valley and Travis Peak sand formations, showing improved performance in pressure fluctuation interpretation and early screenout detection [117]. To address limited data availability in shale gas wells in southeastern Chongqing, Surjaatmadja et al. [118] proposed a pressure-curve-based diagnostic approach. By analyzing pad fluid and main fracturing stages, they qualitatively and quantitatively evaluated rock brittleness and fracture complexity. For example, analysis of Well P revealed: 50% of fractures were planar, 36.4% were complex, and 13.6% showed fracture network behavior. Zhao et al. enhanced Nolte's diagnostic framework by combining pressure trend analysis with real-time slope interpretation, allowing for qualitative identification of fracture propagation patterns [119]. They developed a dynamic segmentation fitting algorithm for bottomhole net pressure curves and proposed a real-time automatic diagnostic method that adjusted parameters based on shale formation characteristics, enabling quantitative evaluation of fracture dynamics under varying pressure regimes. This methodology has been widely applied in national shale gas demonstration zones such as Fuling and Changning-Weiyuan [120].

Another method for fracture identification involves real-time input of treatment data into fracture simulators for history matching and pressure prediction [121]. Crockett developed an integrated three-dimensional hydraulic fracturing model, incorporating four major modules: wellbore fluid flow, fracture propagation, proppant transport, and thermal exchange, all embedded within complex reservoir environments [122]. The model predicted that fracture geometry (length, height, and width) was significantly affected by closure stress differentials: under high stress contrast, fractures were shorter and narrower; proppants primarily accumulated near the wellbore, and the risk of proppant screenout increased with pumping duration.

Subsequently, Crockett improved the model by accounting for asymmetric growth of fracture dimensions over time (length, height, width), incorporating rock mechanical behavior and fluid leak-off dynamics, and integrating real-time monitoring data (e.g., wellhead flow rate, fracturing fluid viscosity, proppant concentration) to optimize fracture geometry prediction [123]. Westwood applied a Monte Carlo method combined with Discrete Fracture Network (DFN) modeling to analyze the impact of pumping parameters (rate, duration, pressure differential) on fracture network area and maximum flow distance in shale gas hydraulic fracturing [124]. When the pressure differential was less than 2 MPa, fracture area decreased significantly with increasing pressure; when the pressure differential exceeded 2 MPa, this effect diminished. The study recommended limiting pressure differential below 2 MPa and shortening pumping duration to reduce lateral fracture propagation. Jenkins employed a modified Theory of Critical Distances (TCD) combined with Von Mises stress analysis to investigate stress field behavior and interactions among multiple fractures during hydraulic fracturing [125]. Cluster spacing was found to decrease with increasing injection pressure and followed a power–law relationship with fracture length. In simulations of three interacting fractures, the central fracture was significantly influenced by stress interference from adjacent fractures, suggesting that cluster spacing should be optimized to prevent fracture coalescence.

With advancements in computing and artificial intelligence, an increasing number of data-driven pressure inversion methods have been proposed [126,127]. However, reliance on a single net pressure curve or fluid leak-off profile may correspond to multiple combinations of fracture geometry and reservoir parameters, leading to non-unique solutions and unreliable production forecasts. This non-uniqueness can mislead fracturing design and reservoir development decisions. Therefore, it is essential to integrate pressure transient testing, radioactive tracer logging, and long-term production monitoring to constrain the solution space and improve inversion accuracy [128].

3.2. Fracture Evaluation Based on Shut-In Water Hammer Curve

Fracture network parameter inversion based on post-shut-in data primarily utilizes the water hammer effect of fluid within fractures after the cessation of injection (Figure 8) [129]. The water hammer effect refers to pressure oscillations in the wellbore caused by abrupt changes in flow rate, commonly observed during shut-in and stage transitions in hydraulic fracturing operations [130]. These pressure pulses propagate down the wellbore, interact with the created fractures, and return to the surface, manifesting as a series of oscillations on the pressure–time curve. The water hammer effect was first proposed as a diagnostic tool in 1985, when Holzhausen and Gooch defined the complex ratio of oscillatory pressure to flow as "fracture impedance," to characterize the fracture's response to fluid perturbations [131]. Through impedance analysis, fracture closure pressure and dimensions can be dynamically evaluated by measuring pressure/flow oscillations [132]. While this technique was originally applied in vertical fractured wells, recent studies have extended its applicability to horizontal wells with multi-stage fracturing.

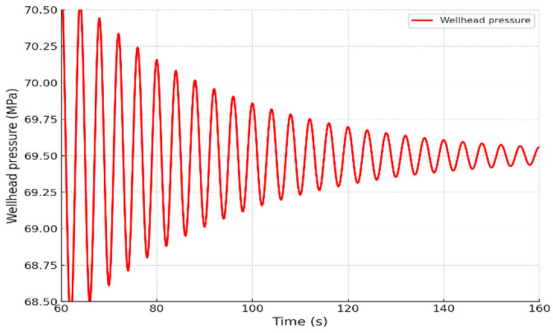


Figure 8. Pump-in Water Hammer Effect.

Ashour (1994) extended Holzhausen's HIT method to both vertical and horizontal hydraulic fractures and demonstrated that fracture length, height, and conductivity could be inverted by analyzing the time delay and amplitude of the reflected wave at the wellhead [133]. Patzek et al. [134] dynamically evaluated fracture state and geometry using transient pressure responses, optimizing the injection process. Their model accurately reproduced the post-step decay pattern, highlighting the sensitivity of response behavior to fracture size. Mondal introduced an equivalent electrical circuit model (R–C–I components) to describe the wellbore–formation interface impedance. Mathematical relationships were established between fracture resistance (R), capacitance (C), inductance (I), and geometric parameters such as half-length, height, and width. Inversion of R–C–I parameters produced results consistent with those from commercial simulators [135]. Carey extracted R, C, and I parameters via history matching of water hammer data and compared them with SRV estimates [136]. Capacitance (C) showed a strong positive correlation with SRV ($r = 0.81$), indicating fracture volume; inductance (I) also had a positive correlation with SRV ($r = 0.75$), supporting the large-fracture-network hypothesis; resistance (R) showed a weak negative correlation with SRV ($r = -0.45$), suggesting near-wellbore friction suppresses fracture propagation. The computed fracture half-length correlated strongly with SRV length ($r = 0.80$). Iriarte analyzed water hammer data from more than 100 wells to assess correlations between signal characteristics and fracturing scale, fluid type, completion method, and well productivity [137]. High attenuation rates were associated with complex fracture networks and significant fluid leak-off, while prolonged signal durations indicated large fracture volumes. Shen modeled the near-well fracture boundary as a series R (resistance)–C (capacitance)–I (inductance) circuit to simulate post-shut-in pressure oscillations [138]. Taking the W2 shale gas block in the Sichuan Basin as an example, MATLAB was used to simulate shut-in pressure oscillations and invert fracture parameters (half-length, height, width). The results showed high agreement with microseismic data. Sensitivity analysis indicated: R reflects fracture volume, C is useful for monitoring stage effectiveness, and I affects fracture width calculations. Hu expanded the single-fracture R-C-I model to multi-fracture scenarios by considering inter-fracture stress interference and conducting sensitivity analyses [139]. Increasing the number of fractures led to a decrease in average fracture length but an increase in total network size. Larger fracture spacing reduced stress interference, minimizing variability in fracture dimensions. A decrease in total fracture volume shifted the water hammer signal downward. Jia employed filtering techniques to denoise shut-in pressure curves. Cepstrum analysis was used to identify negative peaks corresponding to fracture impulse responses. By combining this with wave velocity transformation, fracture depth was calculated. The number of negative peaks matched the actual fracture count [140].

Another method for evaluating artificial fracture networks is the G-function, which was first proposed in 1987 [141]. Castillo plotted the pressure decline value (ΔP) against

the dimensionless time function G (t_0,0) on a Cartesian coordinate system. The intercept of the resulting curve represents the instantaneous shut-in pressure, allowing theoretical estimation of the instantaneous shut-in pressure. Yuan utilized the G-function curve following shut-in to assess fracture complexity [142]. When natural fractures are well-developed, the G-function curve shows a significant upward trend. A straight-line pattern indicates matrix-dominated leak-off, while a high slope reflects elevated matrix permeability. The peak value correlates with the number of fracture branches.

Pressure decline analysis based on injection and shut-in theory can effectively identify the dominant post-fracture flow regime—such as pseudo-homogeneous flow, fracture-dominated flow, or complex fracture network flow. Tu et al. [143] argued that traditional G-function models neglect stress shadowing and dynamic flow redistribution when multiple fractures propagate simultaneously. They introduced the effects of stress superposition and dynamic flow partitioning during multi-fracture closure processes. By combining G-function theory with dynamic multi-fracture closure behavior, the model enables rapid inversion of heterogeneous fracture geometry and is particularly suitable for evaluating hydraulic fracturing in unconventional reservoirs. Jatykov applied the derivative of the G-function, integrating it with lithology logs to identify lithofacies-related closure events [144]. Multi-platform features in the G-function derivative curve reflected closure events across multiple lithofacies. When combined with lithological information, this method allowed for the optimization of fracture height and conductivity design. The sequence of fracture closure was consistent with lithofacies stress contrasts.

Water hammer signals can be used to assess wellbore-to-fracture connectivity, fracture network size, and overall fracturing effectiveness. However, interpretation must consider the effects of completion type, fluid parameters, and reservoir properties [145]. Time-domain analysis of water hammer data often suffers from solution non-uniqueness and cannot reliably diagnose fracture geometry. Incorporating high-frequency data or frequency-domain analysis is essential to enhance resolution [146]. Moreover, G-function permeability reflects the composite response of both fractures and matrix, not matrix permeability alone, leading to increased error under high-permeability or complex fracture network conditions [147].

3.3. Fracture Network Inversion Based on Flowback and Stable Production Data

The evaluation methods applied during the flowback and stable production stages are fundamentally similar, with the key differences lying in flow phase, flow regime, and dominant mechanisms [148]. The flowback stage is typically characterized by single-phase flow of fracturing fluid, dominated by linear flow behavior and mechanisms such as stress sensitivity and gas–water two-phase flow. In contrast, the stable production stage exhibits dual-linear or pseudo-steady-state flow, governed by mechanisms including gas desorption, diffusion, gas–water two-phase flow, stress sensitivity, and rock creep [149,150].

In 1998, Crafton utilized early flowback data to evaluate reservoir parameters and fracturing effectiveness. By applying the Reciprocal Productivity Index (RPI) method in conjunction with semi-log time plots (MDH plots), the product of permeability and thickness (kh) was calculated. The Agarwal–Gringarten type curves were then used to determine the fracture half-length by identifying the endpoint of the fracture-dominated linear flow period [151]. Compared to stable production, flowback periods offer higher-frequency data acquisition. Crafton analyzed high-frequency flowback data ($\geq$20 samples per minute) to evaluate fracture conductivity, effective fracture half-length, near-well matrix permeability, and closure pressure. Results showed that after gas breakthrough, fracture conductivity decreased and effective fracture length shortened significantly. Although high-frequency flowback data (>20 times/minute) can effectively evaluate fracture

parameters, it has not yet become a standard practice in the industry [152]. Clarkson analyzed two-phase flow data during the flowback stage of multi-fractured horizontal wells (MFHWs), assuming that water primarily originated from the main fracture network and gas from adjacent matrix domains. This allowed estimation of fracture permeability and total fracture half-length [153]. Although two-phase flowback analysis enables estimation of fracture parameters, uncertainties remain in parameters such as fracture porosity and relative permeability. Xu developed a two-phase flow model based on material balance, analyzing early gas production mechanisms (water-dominated flow with declining gas–water ratio) to estimate effective fracture volume [154]. During early production, the fracture network behaves as a near-closed system, with gas expansion serving as the main driving force—allowing the fracture volume to be estimated using material balance. Williams improved upon two-phase flow analysis models for MFHWs during flowback by coupling transient linear flow with multiphase depletion in fractures and incorporating dynamic fracture porosity and permeability. This allowed for more accurate estimation of fracture properties (e.g., conductivity, half-length) [155]. Fracture parameters estimated using short-term (∼2 days) flowback data aligned well with those derived from long-term production analysis. Wang developed a multi-mechanism dual-porosity model to study hydraulic fracturing fluid leak-off and flowback behavior [156]. Following fracturing, a high water-saturation zone forms around fractures. Although water saturation declines during flowback, residual water often remains. Xu proposed an open material balance model to analyze fracture volume changes during early flowback (increasing gas–water ratio) and late flowback (decreasing gas–water ratio) [157]. In early flowback, rapid fracture closure leads to significant loss of effective volume, whereas in later stages, support from matrix gas slows the rate of closure. Yang et al. analyzed flowback water volume, chemical composition, and chloride concentration from 19 fractured wells to reveal fracture characteristics [158]. A high flowback rate coupled with low Cl^- concentration indicates wide fractures; conversely, a low flowback rate and high Cl^- suggest narrow fracture systems. Zhang developed a semi-analytical method that combines two-phase flow in fractures and matrix, while accounting for pressure-dependent rock and fluid properties, to analyze shale gas flowback data and evaluate fracture properties [159]. The new method enables accurate quantification of fracture dynamics, though results are sensitive to initial fracture permeability, half-length, and matrix water saturation. He later proposed a semi-analytical decline curve model that simultaneously accounts for two-phase flow in fractures and matrix, as well as variable bottomhole pressure/flow rate conditions [160]. Six synthetic numerical cases (shale gas and shale oil) were used to validate the method, which achieved fracture property estimation errors under 10%.

Domestic and international scholars have developed various fracture models for the stable production stage, primarily based on differences in flow regimes across different shale gas regions. The evolution of flow models in shale gas reservoirs has progressed from the early three-region model to more advanced multi-mechanism coupled composite models.

In early research, the three-region model proposed by Lee and Brockenbrough laid the foundation for flow analysis in vertically fractured wells [161], but it was limited to Darcy flow and did not account for gas desorption characteristics inherent to shale gas. Later, Brown [162] and Stalgorova [163] applied this model to multi-fractured horizontal wells (MFHWs) in tight gas reservoirs, yet they overlooked the productivity contributions from the inter-fracture matrix. Although Stalgorova introduced geometric effects of fracture branching, her model still failed to capture inter-well matrix flow and gas–water interactions. Recognizing the unique behavior of shale gas, Zhao et al. [164] incorporated mass conservation, Darcy's law, and the Langmuir isotherm to account for adsorbed gas desorption in pressure transient analysis. Their findings showed that with more fractures,

early radial flow appears sooner. Qiu solved a triple-porosity model in real space, yielding results consistent with numerical simulations. The model parameters have clear physical significance and allow for estimation of porosity in each region, supporting both history matching and production forecasting [165]. Qiu also proposed a semi-analytical well testing method to evaluate heterogeneous fracture parameters, such as fracture half-length, conductivity, and storage ratio, and further analyzed the correlation between fracturing fluid volume and fracture parameters [166]. The semi-analytical model effectively characterizes heterogeneous fractures, identifies seven flow regimes, and demonstrates strong agreement with field pressure data. Wang applied pressure build-up testing to analyze post-fracture network features in shale gas wells in the Sichuan Basin, establishing a novel interpretation model—the trilinear flow model—for quantitative parameter evaluation [167]. Findings by region included: Fuling main block: complex fracture networks with well-supported secondary fractures; Pingqiao South: moderate fracturing effectiveness; Yongchuan block: low fracture complexity, dominated by main fractures; Wulong area: low formation energy and severe fluid retention. As research has advanced, the traditional three-region model can no longer adequately describe the full complexity of shale gas flow mechanisms under modern development conditions [168].

To address the heterogeneity of complex fracture networks, Stalgorova and Mattar proposed a five-region composite model [169]. This model divides the reservoir into: Main fractures, Secondary fractures, Inter-fracture matrix, Inter-well matrix, Undisturbed zones. It was the first analytical model to quantify permeability contrasts between inter-fracture and inter-well matrix zones. However, the model still had significant limitations: it did not couple two-phase flow equations or stress sensitivity effects, making it unable to simulate dynamic suppression of gas-phase permeability by retained fracturing fluids or the decline in fracture conductivity during production.

Subsequent studies have progressively expanded toward multi-physics field integration:

Deng et al. built upon the five-region model by incorporating non-uniform fracture distribution, varying reservoir properties, and adsorption effects [170]. A sensitivity analysis on fracture dimensions showed: the smaller the SRV (Stimulated Reservoir Volume), the shorter the first linear flow stage; the transition flow appeared earlier. Non-uniform SRV led to pressure responses intermediate between those of the maximum and minimum uniform cases. An increase in fracture number shortened the second linear flow stage and advanced the boundary-dominated flow. Variation in fracture spacing had limited influence on pressure response. Zeng proposed a seven-region composite linear flow model, which considered heterogeneity, multi-mechanism flow, and partial fracture penetration. The reservoir was divided into seven zones: Two upper/lower reservoir layers, Two outer reservoir zones, Two inner reservoir zones, One hydraulic fracture zone. This model was used for transient pressure and production analysis in shale gas reservoirs with multi-fractured horizontal wells [171]. It successfully matched field production data. After accounting for diffusion, slippage, and desorption, the model could effectively predict secondary fracture permeability and hydraulic fracture conductivity. Wu introduced a novel Production Data Analysis (PDA) method to quantify the impact of inter-well fracture connectivity on production dynamics after infill drilling. The method also enabled characterization of fracture parameters. For example, when well spacing was reduced to 300 m, the parent well's production significantly increased, confirming inter-well fracture communication. PDA effectively resolved both near-well SRV and inter-well SRV parameters, validating its practical utility [172]. Cheng proposed a semi-analytical model that quantitatively characterized the dynamic shrinkage of inner boundaries and supporting fractures through a pressure-dependent contraction coefficient. For the first time, this approach enabled quantitative description of the time-dependent shrinkage behavior of inner boundaries and

support fractures, while also identifying distinct features in transient pressure curves [173]. Chen et al. [174] developed a semi-analytical model in which interference between fractures was used to generate typical pressure transient curves. The model showed that increasing the number, length, and conductivity of hydraulic fractures would weaken the "microfracture-hydraulic fracture" effect and reduce pressure drop. In contrast, increasing microfracture attributes (number, length, conductivity) would enhance the coupling effect and increase pressure drop. Li et al. proposed a semi-analytical model that simultaneously considered reservoir heterogeneity, complex fracture geometries, and differences between SRV and unmodified zones [175]. The model predicted transient pressure behavior in complex fracture networks within heterogeneous reservoirs. Increasing fracture count reduced pressure drop and ended the linear flow regime earlier. Cui et al. [176] established a multi-domain, multi-physics model to study two-phase flow in SRV and USRV (Unstimulated Reservoir Volume) regions. The model evaluated the influence of hydraulic fracturing parameters—such as effective stress and proppant loading—on shale gas production. High stress reduced permeability, but proppants (especially in multilayer configurations) mitigated the effects of stress sensitivity. Deng et al. proposed an improved gas–water two-phase flow model to analyze pressure fields, water saturation fields, and production performance of multi-cluster fractured horizontal wells [177]. In the early stage, each cluster exhibited independent outflow; in later stages, they merged into a unified flow region. The formation of high-conductivity channels due to physical contact in tree-like fracture networks significantly influenced pressure and saturation distributions.

Despite these advancements, current models for characterizing hydraulic fractures during the flowback and stable production stages still face several limitations including the following [178,179].

Lack of dynamic multi-physics coupling: most existing models treat individual mechanisms—such as adsorption, stress sensitivity, or gas–water two-phase flow—in isolation. There remains a lack of unified models that dynamically couple these processes across different time and spatial scales. Inadequate representation of flow mechanisms in the stimulated fracture network (SRV).

Most models assume homogeneity when dealing with the stress sensitivity of supported vs. unsupported fractures and the two-phase flow behavior within the SRV. This oversimplification reduces the ability to distinguish between various flow regimes and spatial zones.

Oversimplification of transient multiphase flow during early flowback: complex multiphase flow processes are often reduced to pseudo-single-phase assumptions, which may misrepresent pressure and saturation evolution, particularly during gas breakthrough and fracture closure.

Neglect of horizontal well heterogeneity:

Along the horizontal lateral, significant variations exist in reservoir properties such as porosity, permeability, and adsorbed gas content. However, these heterogeneities are often only partially reflected through cuttings analysis and are not effectively incorporated into dynamic modeling frameworks.

4. Summary of Current Fracture Evaluation Methods and Future Development Trends

Scholars in China and abroad have systematically reviewed the applicability, advantages, and disadvantages of various fracture evaluation methods [180]. In engineering practice, it is essential to select appropriate evaluation approaches based on reservoir geological characteristics, stimulation objectives, and data availability. As shown in Tables 1 and 2, significant differences exist between direct monitoring and dynamic inversion methods

in terms of fracture parameter acquisition capabilities, technical strengths, and limitations [181]. Research has shown that due to their inherent physical principles and data dimensionality constraints, no single method can comprehensively characterize both the geometrical morphology and flow performance of fracture networks. Therefore, multi-method collaborative analysis is urgently needed to improve evaluation accuracy [182].

Table 1. Measurable Parameters, Advantages, and Limitations of Direct Monitoring Methods.

Evaluation Method	Parameters Acquired	Parameters Acquired	Limitations
Microseismic	Fracture half-length, height, azimuth, dip	Non-invasive, real-time fracture evolution tracking	Signal interference susceptibility, geological sensitivity
Tracers	Fracture height, width, length	Intuitive results, multi-medium applicability	Environmental risks, geological/rock property constraints
Wide-Field Electromagnetics	Fracture length, height, cluster efficiency	Non-invasive, deep reservoir applicability	High cost, inversion ambiguity
Distributed Fiber Optics	Fracture volume, length, formation pressure	High sensitivity, multiparameter measurement	High equipment costs, environmental sensitivity
Field Experiments	Fracture width, proppant distribution, conductivity	Detailed parameter insights	Limited scalability, high cost/time

Table 2. Measurable Parameters, Advantages, and Limitations of Dynamic Inversion Methods.

Evaluation Method	Parameters Acquired	Parameters Acquired	Limitations
Fracturing	SRV, fracture area, half-length, conductivity	High-resolution pumping data	Solution non-uniqueness
Shut-in	Closure pressure, fracture complexity	Stage-specific parameter evaluation	Short monitoring duration
Flowback	Fracture volume, half-length, pressure	Single-phase flow simplicity	Underdeveloped mechanistic models
Production	EUR, permeability, fracture parameters	Production history matching	Parameter averaging, flow regime limitations

The strong coupling of fracture parameters (e.g., volume, area, length, height) introduces solution non-uniqueness in single-method inversions. For instance, Clarkson reduced parameter uncertainty by integrating microseismic data (fracture azimuth/complexity) with production logs (effective half-length) [183]. Holly et al. further proposed combining distributed fiber optics and tracers to dynamically calibrate conductivity via temperature–chemical concentration spatial matching [184]. Future trends can be summarized as follows:

1. Multi-Source Data Fusion: Integrate direct monitoring (e.g., microseismic, fiber optics) and dynamic inversion (e.g., flowback curves, production simulations) to build a "geology-engineering-production" unified evaluation framework.
2. AI-Driven Optimization: Leverage machine/deep learning (e.g., CNN-based microseismic signal classification, reinforcement learning for parameter adjustment) to enhance inversion efficiency.
3. High-Resolution Real-Time Monitoring: Develop low-cost distributed fiber sensors and wide-field electromagnetic arrays for minute-level fracture imaging, enabling real-time fracturing optimization.
4. Digital Twin Integration: Combine real-time monitoring with predictive simulations to create virtual replicas of fracturing processes for scenario testing and decision support.

5. Conclusions

This paper systematically reviews the evaluation methodologies for artificial fracture networks in shale gas horizontal wells, encompassing direct monitoring techniques (microseismic, tracers, wide-field electromagnetics, distributed optical fiber, and field experiments) and dynamic inversion approaches (fracturing, shut-in, flowback, and production stages). Research indicates that existing technologies can support fracture network characterization through geometric parameterization and seepage efficiency assessment.

Single evaluation methods, constrained by their inherent principles and data dimensionality, struggle to fully resolve the nonlinear coupling relationships among fracture parameters. Future efforts must emphasize multi-source data fusion (e.g., integrated microseismic–tracer–fiber monitoring) and cross-scale modeling (from nanopores to fracture networks) to construct self-consistent evaluation frameworks, thereby reducing inversion uncertainties.

Artificial intelligence (e.g., machine learning, digital twins) offers novel paradigms for fracture evaluation, yet faces two critical challenges:

Limited Generalization: Sparse training data hinder model adaptability to diverse geological conditions.

Algorithm Robustness: Validation under complex subsurface environments remains insufficient.

Subsequent research should establish standardized verification protocols through field trials and numerical simulations to accelerate the industrial deployment of these technologies. Additionally, integrating multi-physics mechanisms (e.g., adsorption–desorption, stress sensitivity, multiphase flow) into dynamic models will enhance the fidelity of fracture network characterization during flowback and production stages. This work provides theoretical and practical guidance for optimizing fracture evaluation systems in shale gas development, aiming to achieve efficient and sustainable resource utilization.

Author Contributions: Methodology, W.X. and Y.S.; investigation, H.Y., Z.T., W.N. and Y.L.; writing—original draft preparation, H.Y.; writing—review and editing, H.Y.; supervision, W.X. and Y.S. All authors have read and agreed to the published version of the manuscript.

Funding: This research was funded by the China National Petroleum Corporation (CNPC)'s Basic and Foresight-Oriented Science and Technology Program, project "Mechanisms of Shale Oil and Gas Development and Volumetric Development Technology" (Grant No. 2023ZZ08).

Acknowledgments: The authors gratefully acknowledge the support of the National Energy Shale Gas R&D Center for this work.

Conflicts of Interest: The authors declare that this study received funding from China National Petroleum Corporation (CNPC). The funder was not involved in the study design, collection, analysis, interpretation of data, the writing of this article or the decision to submit it for publication.

References

1. Wang, Q.; Chen, X.; Jha, A.N.; Rogers, H. Natural gas from shale formation-the evolution, evidences and challenges of shale gas revolution in United States. *Renew. Sustain. Energy Rev.* **2014**, *30*, 1–28. [CrossRef]
2. Hao, F.; Zou, H.; Lu, Y. Mechanisms of shale gas storage: Implications for shale gas exploration in China. *AAPG Bull.* **2013**, *97*, 1325–1346. [CrossRef]
3. Tang, Y.; Tang, X.; Wang, G.Y.; Zhang, Q. Summary of hydraulic fracturing technology in shale gas development. *Geol. Bull. China* **2011**, *30*, 393–399.
4. Liu, Z.; Wang, T.; Gao, Y.; Zeng, Q.; Zhuang, Z.; Huang, K.C. The key mechanical problems on hydraulic fracture in shale. *Guti Lixue Xuebao/Acta Mech. Solida Sin.* **2016**, *37*, 34–49. [CrossRef]
5. Liu, Y.; Yang, H.; Zhang, Q.; Xiong, D. Properties of a shale bedding plane and its influence on the geometric parameters of fracture propagation in volume fracturing. *Eng. Fract. Mech.* **2022**, *266*, 108413. [CrossRef]

6. Wright, C.A.; Weijers, L.; Davis, E.J.; Mayerhofer, M. Understanding hydraulic fracture growth: Tricky but not hopeless. In Proceedings of the SPE Annual Technical Conference and Exhibition, Houston, TX, USA, 3–6 October 1999; p. SPE-56724. [CrossRef]
7. Ren, L.; Su, Y.; Zhan, S.; Meng, F. Progress of the research on productivity prediction methods for stimulated reservoir volume (SRV)-fractured horizontal wells in unconventional hydrocarbon reservoirs. *Arab. J. Geosci.* **2019**, *12*, 184. [CrossRef]
8. King, G.E. Hydraulic fracturing 101: What every representative, environmentalist, regulator, reporter, investor, university researcher, neighbor and engineer should know about estimating frac risk and improving frac performance in unconventional gas and oil wells. In Proceedings of the SPE Hydraulic Fracturing Technology Conference and Exhibition, Woodlands, TX, USA, 6–8 February 2012; p. SPE-152596. [CrossRef]
9. Mueller, M. Meeting the challenge of uncertainty in surface microseismic monitoring. *First Break* **2013**, *31*. [CrossRef]
10. Cipolla, C.; Maxwell, S.; Mack, M. Engineering guide to the application of microseismic interpretations. In Proceedings of the SPE Hydraulic Fracturing Technology Conference and Exhibition, Woodlands, TX, USA, 6–8 February 2012; p. SPE-152165. [CrossRef]
11. Shu, H.; Dawod, A.Y. Microseismic Monitoring Signal Waveform Recognition and Classification: Review of Contemporary Techniques. *Appl. Sci.* **2023**, *13*, 12739. [CrossRef]
12. Van Der Baan, M.; Eaton, D.; Dusseault, M. Microseismic monitoring developments in hydraulic fracture stimulation. In Proceedings of the ISRM International Conference for Effective and Sustainable Hydraulic Fracturing, Brisbane, Australia, 20 May 2013; p. ISRM-ICHF. [CrossRef]
13. Maxwell, S.C.; Rutledge, J.; Jones, R.; Fehler, M. Petroleum reservoir characterization using downhole microseismic monitoring. *Geophysics* **2010**, *75*, A129–A175. [CrossRef]
14. Clarkson, C.R.; Aguilera, R.; Pedersen, P.K.; Spencer, R.J. Shale gas, part 8: Shale gas development optimization. *CSPG Reserv.* **2011**, *38*, 25–31.
15. Maxwell, S.C.; Raymer, D.; Williams, M.; Primiero, P. Tracking microseismic signals from the reservoir to surface. *Lead. Edge* **2012**, *31*, 1300–1308. [CrossRef]
16. Furong, W.; Yan, Y.; Yin, C. Real-time microseismic monitoring technology for hydraulic fracturing in shale gas reservoirs: A case study from the Southern Sichuan Basin. *Nat. Gas Ind. B* **2017**, *4*, 68–71. [CrossRef]
17. Li, L.; Tan, J.; Wood, D.A.; Zhao, Z.; Becker, D.; Lyu, Q.; Chen, H. A review of the current status of induced seismicity monitoring for hydraulic fracturing in unconventional tight oil and gas reservoirs. *Fuel* **2019**, *242*, 195–210. [CrossRef]
18. Duncan, P.M. Microseismic monitoring: Technology state of play. In Proceedings of the SPE Unconventional Resources Conference/Gas Technology Symposium, Pittsburgh, PA, USA, 23–25 February 2010; p. SPE-131777. [CrossRef]
19. Eisner, L.; Duncan, P.M.; Heigl, W.M.; Keller, W.R. Uncertainties passive seismic monitoring. *Lead. Edge* **2009**, *28*, 648–655. [CrossRef]
20. Peyret, O.; Drew, J.; Mack, M.; Brook, K.; Maxwell, S.; Cipolla, C. Subsurface to surface microseismic monitoring for hydraulic fracturing. In Proceedings of the SPE Annual Technical Conference and Exhibition, San Antonio, TX, USA, 8–10 October 2012; p. SPE-159670. [CrossRef]
21. Warpinski, N.R.; Wolhart, S. A validation assessment of microseismic monitoring. In Proceedings of the SPE Hydraulic Fracturing Technology Conference and Exhibition, Woodlands, TX, USA, 9–11 February 2016; p. D021S004R001. [CrossRef]
22. Maxwell, S. Microseismic: Growth born from success. *Lead. Edge* **2010**, *29*, 338–343. [CrossRef]
23. Warpinski, N.R.; Du, J.; Zimmer, U. Measurements of hydraulic-fracture-induced seismicity in gas shales. *SPE Prod. Oper.* **2012**, *27*, 240–252. [CrossRef]
24. Zhao, J.; Ren, L.; Lin, C.; Lin, R.; Hu, D.; Wu, J.; Jiang, H. A review of deep and ultra-deep shale gas fracturing in China: Status and directions. *Renew. Sustain. Energy Rev.* **2025**, *209*, 11511. [CrossRef]
25. Shemeta, J.; Anderson, P. It's a matter of size: Magnitude and moment estimates for microseismic data. *Lead. Edge* **2010**, *29*, 296–302. [CrossRef]
26. Maxwell, S.; Zimmer, U.; Warpinski, N.; Waltman, C. Quality control/assurance reporting of passive microseismic data. In Proceedings of the SEG International Exposition and Annual Meeting, New Orleans, LA, USA, 1–6 October 2006; p. SEG-2006. [CrossRef]
27. Dwan, F.; Qiu, J.; Zhou, M.; Yuan, R.S.; Zhang, Z. Sichuan shale gas microseismic monitoring: Acquisition, processing, and integrated analyses. In Proceedings of the International Petroleum Technology Conference, Beijing, China, 26–28 March 2013; p. IPTC-16571. [CrossRef]
28. Mahmoud, A.; Gowida, A.; Aljawad, M.S.; Al-Ramadan, M.; Ibrahim, A.F. Advancement of hydraulic fracture diagnostics in unconventional formations. *Geofluids* **2021**, *2021*, 4223858. [CrossRef]
29. Webster, P.; Cox, B.; Molenaar, M. Developments in diagnostic tools for hydraulic fracture geometry analysis. In Proceedings of the Unconvenional Resources Technology Conference, Denver, CO, USA, 12–14 August 2013; pp. 218–224. [CrossRef]

30. Sani, A.M.; Podhoretz, S.B.; Chambers, B.D. The use of completion diagnostics in Haynesville shale horizontal wells to monitor fracture propagation, well communication, and production impact. In *SPE Canada Unconventional Resources Conference*; SPE: Richardson, TX, USA, 2015; p. D021S006R002.
31. Palisch, T.; Al-Tailji, W.; Bartel, L.; Cannan, C.; Czapski, M.; Lynch, K. Recent advancements in far-field proppant detection. In Proceedings of the SPE Hydraulic Fracturing Technology Conference and Exhibition, Woodlands, TX, USA, 9–11 February 2016; p. D021S006R007. [CrossRef]
32. Zhang, J.; Smith, H.; Palisch, T.; Reynaud, L. A Novel Technology for Locating and Evaluating Hydraulic Fractures in Horizontal Wells-Modeling and Field Results. In Proceedings of the SPE Annual Technical Conference and Exhibition, Dallas, TX, USA, 24–26 September 2018; p. D011S004R003. [CrossRef]
33. Dugstad, O. Well to Well Tracer Tests, Chapter 6, Reservoir Engineering and Petrophysics. *Pet. Eng. Handb.* **2007**, *651*. [CrossRef]
34. Salman, A.; Kurtoglu, B.; Kazemi, H. Analysis of Chemical Tracer Flowback in Unconventional Reservoirs. In Proceedings of the SPE/CSUR Unconventional Resources Conference, Calgary, AB, Canada, 30 September–2 October 2014. [CrossRef]
35. Li, G. Oilfield Tracer Analysis and Application for Hydraulic Fracture Diagnostics. Ph.D. Dissertation, Texas A&M University, San Antonio, TX, USA, May 2021.
36. Du, Y.; Guan, L. Interwell tracer tests: Lessons learned from past field studies. In Proceedings of the SPE Asia Pacific Oil and Gas Conference and Exhibition, Jakarta, Indonesia, 5–7 April 2005; p. SPE-93140. [CrossRef]
37. Aparecida de Melo, M.; de Holleben, C.R.; Almeida, A.R. Using tracers to characterize petroleum reservoirs: Application to Carmopolis Field, Brazil. In Proceedings of the SPE Latin America and Caribbean Petroleum Engineering Conference, Buenos Aires, Argentina, 25 March 2001; p. SPE-69474. [CrossRef]
38. Mercado, M.; Perez, C.E.; Asadi, M.; Casas, D.R. Gas flood-flow pattern evaluation: A successful interwell field study. In Proceedings of the SPE Latin America and Caribbean Petroleum Engineering Conference, Port of Spain, Trinidad and Tobago, 27 April 2003; p. SPE-81005. [CrossRef]
39. Kumar, A.; Seth, P.; Shrivastava, K.; Manchanda, R.; Sharma, M.M. Integrated analysis of tracer and pressure-interference tests to identify well interference. *SPE J.* **2020**, *25*, 1623–1635. [CrossRef]
40. Li, H.; Liu, Z.; Li, Y.; Luo, H.; Cui, X.; Nie, S.; Ye, K. Evaluation of the release mechanism of sustained-release tracers and its application in horizontal well inflow profile monitoring. *ACS Omega* **2021**, *6*, 19269–19280. [CrossRef] [PubMed]
41. Katashov, A.; Belova, A.; Husein, N.; Drobot, A.; Upadhye, V.; Stepanova, M.; Vasechkin, D. Tracer-Based Technology for Evaluation the Productivity of Frac Ports and the Contribution of Near and Far Zones of Fractures During Hydraulic Stimulation. In Proceedings of the Offshore Technology Conference, Houston, TX, USA, 2–5 May 2022; p. D031S039R006. [CrossRef]
42. Roshan, H.; Sarmadivaleh, M.; Iglauer, S. Shale fracture surface area measured by tracking exchangeable cations. *J. Pet. Sci. Eng.* **2016**, *138*, 97–103. [CrossRef]
43. Lal, M.K.; Singh, A.K.; Ezernack, J.; Spencer, J. Advanced reservoir characterization in antelope shale using chemical tracer technology. In Proceedings of the SPE Hydraulic Fracturing Technology Conference and Exhibition, Woodlands, TX, USA, 24 January 2017; p. D011S001R007. [CrossRef]
44. Brigham, W.E.; Smith, D.H., Jr. Prediction of tracer behavior in five-spot flow. In Proceedings of the SPE Conference on Production Research and Engineering, Tulsa, OK, USA, 3 May 1965; p. SPE-1130. [CrossRef]
45. Abbaszadeh-Dehghani, M.; Brigham, W.E. Analysis of well-to-well tracer flow to determine reservoir layering. *J. Pet. Technol.* **1984**, *36*, 1753–1762. [CrossRef]
46. Jensen, C.L.; Horne, R.N. *Matrix Diffusion and Its Effect on the Modeling of Tracer Returns from the Fractured Geothermal Reservoir at Wairakei, New Zealand (No. SGP-TR-74-43)*; Stanford University: Palo Alto, CA, USA, 1983.
47. Rivera, J.R.; Ramirez, J.S.; Rodriguez, F.G. *Parallel Fractures Model for Tracer Flow Through Geothermal Reservoirs-Preliminary Results*; Stanford University: Stanford, CA, USA, 20–22 January 1987.
48. Tian, W.; Wu, X.; Shen, T.; Kalra, S. Estimation of hydraulic fracture volume utilizing partitioning chemical tracer in shale gas formation. *J. Nat. Gas Sci. Eng.* **2016**, *33*, 1069–1077. [CrossRef]
49. Kumar, A.; Sharma, M.M. Diagnosing hydraulic fracture geometry, complexity, and fracture wellbore connectivity using chemical tracer flowback. *Energies* **2020**, *13*, 5644. [CrossRef]
50. Holditch, S.A.; Holcomb, D.L.; Rahim, Z. Using tracers to evaluate propped fracture width. In Proceedings of the SPE Eastern Regional Meeting, Pittsburgh, PA, USA, 2 November 1993; p. SPE-26922. [CrossRef]
51. Lange, A.; Bouzian, J.; Bourbiaux, B. Tracer-test simulation on discrete fracture network models for the characterization of fractured reservoirs. In Proceedings of the SPE Europec featured at EAGE Conference and Exhibition, Madrid, Spain, 13 June 2005; p. SPE-94344. [CrossRef]
52. Ghods, P.; Zhang, D. Automatic estimation of fracture properties in multi-stage fractured shale gas horizontal wells for reservoir modeling. In Proceedings of the SPE Western Regional Meeting, Bakersfield, CA, USA, 19–23 March 2012; p. SPE-153913. [CrossRef]

53. Elahi, S.H.; Jafarpour, B. Characterization of fracture length and conductivity from tracer test and production data with Ensemble Kalman filter. In Proceedings of the Unconventional Resources Technology Conference, San Antonio, TX, USA, 20–22 July 2015; pp. 1192–1200. [CrossRef]
54. Elahi, S.H.; Jafarpour, B. Dynamic fracture characterization from tracer-test and flow-rate data with ensemble Kalman filter. *SPE J.* **2018**, *23*, 449–466. [CrossRef]
55. Liu, J.; Jiang, L.; Liu, T.; Yang, D. Modeling tracer flowback behaviour for a multifractured horizontal well in a tight oil reservoir using the embedded discrete fracture model. *J. Pet. Sci. Eng.* **2022**, *212*, 110347. [CrossRef]
56. Bhatnagar, A. Overcoming challenges in fracture stimulation through advanced fracture diagnostics. In Proceedings of the SPE Asia Pacific Hydraulic Fracturing Conference, Beijing, China, 24 August 2016; p. D021S004R005. [CrossRef]
57. Bartuska, J.E.; Pechiney, J.J.; Leonard, R.S.; Woodroof, R.A. Optimizing completion designs for horizontal shale gas wells using completion diagnostics. In Proceedings of the SPE Unconventional Resources Conference/Gas Technology Symposium, Pittsburgh, PA, USA, 5 June 2012; p. SPE-155759. [CrossRef]
58. Warpinski, N.R. Hydraulic fracture diagnostics. *J. Pet. Technol.* **1996**, *48*, 907–910. [CrossRef]
59. Lichtenberger, G.J. Field applications of interwell tracers for reservoir characterization of enhanced oil recovery pilot areas. In Proceedings of the SPE Oklahoma City Oil and Gas Symposium/Production and Operations Symposium, Oklahoma, OK, USA, 7 April 1991; p. SPE-21652. [CrossRef]
60. He, J.-S. Wide field electromagnetic method and pseudo random signal method. *J. Cent. South Univ. Sci. Technol.* **2010**, *41*, 1065–1072.
61. He, J.-S.; Yang, Y.; Li, D.-Q.; Weng, J.-B. Wide field electromagnetic sounding methods. In Proceedings of the Symposium on the Application of Geophysics to Engineering and Environmental Problems, Austin, TX, USA, 22–26 March 2015; pp. 325–329. [CrossRef]
62. He, J.-S. Combined application of wide-field electromagnetic method and flow field fitting method for high-resolution exploration: A case study of the Anjialing No. 1 Coal Mine. *Engineering* **2018**, *4*, 667–675. [CrossRef]
63. Liu, R.; Liu, J.; Liu, C.; Guo, R.; Wang, H.; Liu, Z. A feasibility study of the wide-field electromagnetic method for hidden ore deposits prospecting. *J. Appl. Geophys.* **2020**, *179*, 104121. [CrossRef]
64. Yuan, B.; Li, D.; Bayless, R.C. Wide field electromagnetic method for shale gas exploration in southern China: A case study. *J. Environ. Eng. Geophys.* **2017**, *22*, 279–289. [CrossRef]
65. Yang, X.L.; Li, B.; Peng, C.S.; Yang, Y. Application of a wide-field electromagnetic method to shale gas exploration in South China. *Appl. Geophys.* **2017**, *14*, 441–448. [CrossRef]
66. Xie, W.B.; Jiang, Q.Y.; Li, D.Q.; Zhang, Q.X.; Pei, J. Interpolation analysis of electromagnetic real-time monitoring data for hydraulic fracturing based on random forest. *China Sci. Technol. Inf.* **2020**, *12*, 88–89.
67. Yang, J.; Liu, Y. Application of wide-field electromagnetic method in fracturing monitoring of deep shale horizontal wells in Huang 202 well area. *China Pet. Chem. Stand. Qual.* **2023**, *4*, 130–132.
68. Ye, Z.Q.; Fan, Q.H.; Xu, Y.J.; Lu, F.B.; Xiao, W.L. Application of wide-field electromagnetic method in shale gas fracturing monitoring in southern Sichuan. In Proceedings of the 33rd National Natural Gas Academic Annual Conference (2023) V: New Energy and Energy Conservation, Guangxi, China, 1–2 June 2023; pp. 108–113.
69. Hu, Z.F.; Luo, W.F.; Wang, S.J.; Kang, H.X.; Zhou, H.; Zhang, Y.X.; Zhan, S.Q. Application of wide-field electromagnetic method in fracturing monitoring of well Anye-2. *Geophys. Geochem. Explor.* **2023**, *47*, 718–725. [CrossRef]
70. Tie, J.; Zhang, Y.; Cheng, X. Application effectiveness of wide-field electromagnetic method fracturing monitoring technology in Xinjiang region. In Proceedings of the 2024 International Conference on Oil and Gas Field Exploration and Development, Volume I, Shanxi, China, 12–14 September 2024; pp. 1054–1064. [CrossRef]
71. He, J.-S. New advances in the theory and applications of wide-field electromagnetic method. *Geophys. Geochem. Explor.* **2020**, *44*, 985–990.
72. Karaman, O.S.; Kutlik, R.L.; Kluth, E.L. A field trial to test fiber optic sensors for downhole temperature and pressure measurements, West Coalinga Field, California. In Proceedings of the SPE Western Regional Meeting, Anchorage, AK, USA, 22 May 1996; p. SPE-35685. [CrossRef]
73. Nath, D.K.; Finley, D.B.; Kaura, J.D.; Krismartopo, B.; Yudhiarto, W. Real-time fiber-optic distributed temperature sensing (DTS)—New applications in the oil field. In Proceedings of the SPE Annual Technical Conference and Exhibition, San Antonio, TX, USA, 24 September 2006; p. SPE-103069. [CrossRef]
74. Nath, F.; Hoque, S.S.; Mahmood, M.N. Recent advances and new insights of fiber optic techniques in fracture diagnostics used for unconventional reservoirs. In Proceedings of the Unconventional Resources Technology Conference, Denver, CO, USA, 13–15 June 2023; pp. 2276–2295. [CrossRef]
75. Rogers, A. Distributed optical-fibre sensing. *Meas. Sci. Technol.* **1999**, *10*, R75. [CrossRef]
76. Hartog, A.H. *An Introduction to Distributed Optical Fibre Sensors*; CRC Press: Boca Raton, FL, USA, 2017. [CrossRef]

77. Li, H.; Luo, H.; Xiang, Y.; Li, Y.; Jiang, B.; Cui, X.; Gao, S.; Zou, S.; Xin, Y. DTS based hydraulic fracture identification and production profile interpretation method for horizontal shale gas wells. *Nat. Gas Ind. B* **2021**, *8*, 494–504. [CrossRef]
78. Holley, E.H.; Kalia, N. Fiber-optic monitoring: Stimulation results from unconventional reservoirs. In Proceedings of the Unconventional Resources Technology Conference, San Antonio, TX, USA, 20–22 July 2015; pp. 300–315. [CrossRef]
79. Hartog, A. A distributed temperature sensor based on liquid-core optical fibers. *J. Light. Technol.* **1983**, *1*, 498–509. [CrossRef]
80. Tabatabaei, M.; Zhu, D. Fracture-stimulation diagnostics in horizontal wells through use of distributed-temperature-sensing technology. *SPE Prod. Oper.* **2012**, *27*, 356–362. [CrossRef]
81. Tarrahi, M.; Gildin, E.; Moreno, J.; Gonzales, S. Dynamic integration of DTS data for hydraulically fractured reservoir characterization with the ensemble Kalman filter. In Proceedings of the SPE Trinidad and Tobago Section Energy Resources Conference, Port of Spain, Trinidad and Tobago, 9 June 2014; p. D031S018R003. [CrossRef]
82. Yoshida, N.; Zhu, D.; Hill, A.D. Temperature-prediction model for a horizontal well with multiple fractures in a shale reservoir. *SPE Prod. Oper.* **2014**, *29*, 261–273. [CrossRef]
83. Kalia, N.; Gorgi, S.; Holley, E.; Cullick, A.S.; Jones, T. Wellbore Monitoring in Unconventional Reservoirs: Value of Accurate DTS Interpretation and Risks Involved. In Proceedings of the SPE Unconventional Resources Conference/Gas Technology Symposium, Woodlands, TX, USA, 1 April 2014; p. D031S007R003. [CrossRef]
84. Cui, J.; Zhu, D.; Jin, M. Diagnosis of production performance after multistage fracture stimulation in horizontal wells by downhole temperature measurements. *SPE Prod. Oper.* **2016**, *31*, 280–288. [CrossRef]
85. Sun, H.; Yu, W.; Sepehrnoori, K. A new comprehensive numerical model for fracture diagnosis with distributed temperature sensing DTS. In Proceedings of the SPE Annual Technical Conference and Exhibition, San Antonio, TX, USA, 9–11 October 2017; p. D011S002R002. [CrossRef]
86. Ashry, I.; Mao, Y.; Wang, B.; Hveding, F.; Bukhamsin, A.Y.; Ng, T.K.; Ooi, B.S. A review of distributed fiber-optic sensing in the oil and gas industry. *J. Light. Technol.* **2022**, *40*, 1407–1431. [CrossRef]
87. Jin, G.; Roy, B. Hydraulic-fracture geometry characterization using low-frequency DAS signal. *Lead. Edge* **2017**, *36*, 975–980. [CrossRef]
88. Sherman, C.S.; Mellors, R.J.; Morris, J.P. Subsurface monitoring via physics-informed deep neural network analysis of das. In Proceedings of the ARMA US Rock Mechanics/Geomechanics Symposium, New York, NY, USA, 23–26 June 2019; p. ARMA-2019.
89. Titov, A.; Binder, G.; Jin, G.; Tura, A.; Aaron, P.; Yates, M.; Gunnell, A. Analysis of scattered waves observed in inter-stage DAS VSP data from zipper-fracturing operations. In *SEG Technical Program Expanded Abstracts*; Society of Exploration Geophysicists: Houston, TX, USA, 2020; pp. 3793–3797. [CrossRef]
90. Li, X.; Zhang, J.; Grubert, M.; Laing, C.; Chavarria, A.; Cole, S.; Oukaci, Y. Distributed acoustic and temperature sensing applications for hydraulic fracture diagnostics. In Proceedings of the SPE Hydraulic Fracturing Technology Conference and Exhibition, Woodlands, TX, USA, 4–6 February 2020; p. D021S004R003. [CrossRef]
91. Shang, Y.; Sun, M.; Wang, C.; Yang, J.; Du, Y.; Yi, J.; Ni, J. Research progress in distributed acoustic sensing techniques. *Sensors* **2020**, *22*, 6060. [CrossRef]
92. Wang, Y.; Wu, Z.; Wang, F. Research progress of applying distributed fiber optic measurement technology in hydraulic fracturing and production monitoring. *Energies* **2020**, *15*, 7519. [CrossRef]
93. Richards, J.; Bartlett, R.; Onen, D.; Crowther, G.; Molenaar, M.M.; Reynolds, A.; Berlang, W. Cloud-Based Solution for Permanent Fiber-Optic DAS Flow Monitoring. In Proceedings of the SPE Digital Energy Conference and Exhibition, The Woodlands, TX, USA, 3–5 March 2015; p. D031S018R001. [CrossRef]
94. Sui, W.; Liu, R.; Cui, K. Application and research progress of distributed optical fiber acoustic sensing monitoring for hydraulic fracturing. *Sci. Sin. Technol.* **2021**, *51*, 371–387. [CrossRef]
95. Courtier, J.; Chandler, K.; Gray, D.; Martin, S.; Thomas, R.; Wicker, J.; Ciezobka, J. Best practices in designing and executing a comprehensive hydraulic fracturing test site in the Permian Basin. In Proceedings of the SPE/AAPG/SEG Unconventional Resources Technology Conference, Austin, TX, USA, 24–26 July 2017; p. URTEC-2697483. [CrossRef]
96. Curth, P.J.; Courtier, J.R.; Smallwood, G.B.; Mauro, R.; Evans, S. Earth model assists Permian asset valuation. *Oil Gas J.* **2015**, *113*, 64–69.
97. Courtier, J.; Wicker, J.; Jeffers, T. Optimizing the development of a stacked continuous resource play in the Midland basin. In Proceedings of the SPE/AAPG/SEG Unconventional Resources Technology Conference, San Antonio, TX, USA, 1–3 August 2016; p. URTEC-2461811. [CrossRef]
98. Heidbach, O.; Rajabi, M.; Cui, X.; Fuchs, K.; Müller, B.; Reinecker, J.; Reiter, K.; Tingay, M.; Wenzel, F.; Xie, F.; et al. World stress map database release 2016. *Tectonophysics* **2016**, *744*, 484–498. [CrossRef]
99. Trowbridge, S.; Wicker, J.; Courtier, J.; Fairfield, R.; Campbell, T. Application of microseismic to assess hydraulic fracture behavior in relation to completion design and landing zone. In Proceedings of the SPE/AAPG/SEG Unconventional Resources Technology Conference, Austin, TX, USA, 24–26 July 2017; p. URTEC-2674376. [CrossRef]

100. Gale, J.F.; Elliott, S.J.; Laubach, S.E. Hydraulic fractures in core from stimulated reservoirs: Core fracture description of HFTS slant core, Midland Basin, West Texas. In Proceedings of the Unconventional Resources Technology Conference, Houston, TX, USA, 23–25 July 2018; pp. 1340–1357. [CrossRef]
101. Maity, D.; Ciezobka, J. An interpretation of proppant transport within the stimulated rock volume at the hydraulic-fracturing test site in the Permian Basin. *SPE Reserv. Eval. Eng.* **2019**, *22*, 477–491. [CrossRef]
102. Li, T.; Chu, W.; Leonard, P.A. Analysis and interpretations of pressure data from the hydraulic fracturing test site (HFTS). In Proceedings of the Unconventional Resources Technology Conference, Denver, CO, USA, 22–24 July 2019; pp. 2923–2938. [CrossRef]
103. Maity, D.; Ciezobka, J. A data analytics framework for cored fracture imaging and novel characterization workflow-application on samples from Hydraulic Fracturing Test Site HFTS in the Midland Basin. In Proceedings of the SPE Hydraulic Fracturing Technology Conference and Exhibition, The Woodlands, TX, USA, 4–6 February 2020; p. D011S001R005. [CrossRef]
104. Salahshoor, S.; Maity, D.; Ciezobka, J. Stage-level data integration to evaluate the fracturing behavior of horizontal wells at the Hydraulic Fracturing Test Site (HFTS): An insight into the production performance. In Proceedings of the SPE/AAPG/SEG Unconventional Resources Technology Conference, Virtual, 20–22 July 2020; p. D033S074R003. [CrossRef]
105. Salahshoor, S. Analysis and Interpretation of Multi-Source Data at the Hydraulic Fracturing Test Site: A Data-Driven Approach to Improve Well Performance Evaluation in Heterogeneous Formations. In Proceedings of the Latin America Unconventional Resources Technology Conference, Virtual, 16–18 November 2020; pp. 252–262. [CrossRef]
106. Ciezobka, J.; Reeves, S. Overview of hydraulic fracturing test sites (HFTS) in the Permian Basin and summary of selected results (HFTS-I in Midland and HFTS-II in Delaware). In Proceedings of the Latin America Unconventional Resources Technology Conference, Virtual, 16–18 November 2020; pp. 93–102. [CrossRef]
107. Ciezobka, J. Overview of hydraulic fracturing test site 2 in the Permian Delaware Basin (HFTS-2). In Proceedings of the Unconventional Resources Technology Conference, Houston, TX, USA, 26–28 July 2021; pp. 259–278. [CrossRef]
108. Gale, J.F.W.; Elliott, S.J.; Rysak, B.G.; Ginn, C.L.; Zhang, N.; Myers, R.D.; Laubach, S.E. Fracture description of the HFTS-2 slant core, Delaware Basin, West Texas. In Proceedings of the Unconventional Resources Technology Conference, Houston, TX, USA, 26–28 July 2021; pp. 1122–1133. [CrossRef]
109. Zhishuai, Z.; James, D.; Bevc Dimitri, N.; Tan, I.L.C.; Swafford, Y.; Laura Craven, M.; Vissotski, A. Hydraulic Fracture Characterization by Integrating Multidisciplinary Data from the Hydraulic Fracturing Test Site 2 (HFTS-2). In Proceedings of the SPE/AAPG/SEG Unconventional Resources Technology Conference, Houston, TX, USA, 26–28 July 2021. [CrossRef]
110. Bessa, F.; Jerath, K.; Ginn, C.; Johnston, P.; Zhao, Y.; Brown, T.; Sahni, V. Subsurface characterization of hydraulic fracture test site-2 (HFTS-2), Delaware basin. In Proceedings of the Unconventional Resources Technology Conference, Houston, TX, USA, 26–28 July 2021; pp. 241–258. [CrossRef]
111. Pudugramam, V.S.; Zhao, Y.; Bessa, F.; Li, J.; Zakhour, N.; Brown, T.; Sahni, V. Analysis and Integration of the Hydraulic Fracturing Test Site-2 (HFTS-2) Comprehensive Dataset. In Proceedings of the Unconventional Resources Technology Conference, Houston, TX, USA, 26–28 July 2021; pp. 1562–1578. [CrossRef]
112. Liu, X.; Tan, Y.; Singh, A.; Waddle, R.; Hilarides, K.; Forand, D.; Rijken, M. Learnings on fracture and geomechanical modeling from the hydraulic fracturing test site in the Midland Basin, West Texas. In Proceedings of the Asia Pacific Unconventional Resources Technology Conference, Virtual, 16–18 November 2021; pp. 416–442. [CrossRef]
113. Cao, M.; Zheng, S.; Elliott, B.; Sharma, M. Impact of complex fracture networks on well productivity: A case study of the hydraulic fracturing test site# 2. In Proceedings of the SPE Hydraulic Fracturing Technology Conference and Exhibition, The Woodlands, TX, USA, 1–3 February 2022; p. D011S001R002. [CrossRef]
114. Nolte, K.G.; Smith, M.B. Interpretation of fracturing pressures. *J. Pet. Technol.* **1981**, *33*, 1767–1775. [CrossRef]
115. Nolte, K.G. Determination of fracture parameters from fracturing pressure decline. In Proceedings of the SPE Annual Technical Conference and Exhibition, Las Vegas, NV, USA, 23–26 September 1979; p. SPE-8341. [CrossRef]
116. Pirayesh, E.; Soliman, M.Y.; Rafiee, M. Make Decision on the Fly: A New Method to Interpret Pressure-Time Data During Fracturing-Application to Frac Pack. In Proceedings of the SPE Annual Technical Conference and Exhibition, New Orleans, LA, USA, 30 September 2013. [CrossRef]
117. Al-Husain, H.M.; Soliman, M.Y.; Stegent, N.A. Application of moving reference point MRP method to cotton valley and travis peak sand fracturing treatments. In Proceedings of the SPE Hydraulic Fracturing Technology Conference and Exhibition, The Woodlands, TX, USA, 24–26 January 2017; p. D021S005R006. [CrossRef]
118. Surjaatmadja, J.B.; Stephenson, S.; Bhaumik, C.; Thompson, S.; Cheng, A. Analysis of generated and reflected pressure waves during fracturing reveals fracture behavior. In Proceedings of the SPE Annual Technical Conference and Exhibition, San Antonio, TX, USA, 29 September 2002; p. SPE-77598. [CrossRef]
119. Zhao, J.; Ren, L.; Jiang, T.; Hu, D.; Wu, L.; Wu, J.; Du, L. Ten years of gas shale fracturing in China: Review and prospect. *Nat. Gas Ind. B* **2022**, *9*, 158–175. [CrossRef]

120. Zhao, J.; Ren, L.; Lin, R.; Li, K.; Li, Y. Automatic Diagnosis Method for Wellhead Pressure Curve of Hydraulic Fracturing in Shale Gas Horizontal Well. U.S. Patent No. 10,689,972, 23 June 2020.
121. Martinez, A.D.; Wright, C.A.; Wright, T.B. Field Application of Real-Time Hydraulic Fracturing Analysis. In Proceedings of the SPE Rocky Mountain Petroleum Technology Conference/Low-Permeability Reservoirs Symposium, Denver, CO, USA, 26–28 April 1993; p. SPE-25916. [CrossRef]
122. Crockett, A.R.; Okusu, N.M.; Cleary, M.P. A complete integrated model for design and real-time analysis of hydraulic fracturing operations. In Proceedings of the SPE Western Regional Meeting, Oakland, CA, USA, 2–4 April 1986; p. SPE-15069. [CrossRef]
123. Crockett, A.R.; Willis, R.M., Jr.; Cleary, M.P. Improvement of hydraulic fracture predictions by real-time history matching on observed pressures. *SPE Prod. Eng.* **1989**, *4*, 408–416. [CrossRef]
124. Westwood, R.F.; Toon, S.M.; Cassidy, N.J. A sensitivity analysis of the effect of pumping parameters on hydraulic fracture networks and local stresses during shale gas operations. *Fuel* **2017**, *203*, 843–852. [CrossRef]
125. Jenkins, A.; Fathi, E.; Belyadi, F. Stress field behavior induced by hydraulic fracture in shale reservoirs: A practical view on cluster spacing. *J. Nat. Gas Sci. Eng.* **2017**, *48*, 186–196. [CrossRef]
126. Hoda, S.; Iriarte, J. Robust Event Recognition in Real-Time Hydraulic Fracturing Data for Live Reporting and Analysis. In Proceedings of the Unconventional Resources Technology Conference, Virtual, 20–22 July 2020; pp. 3398–3415. [CrossRef]
127. Zhukova, K.; Antonic, M.; Soleša, M.; Camber, D. Data-Driven Model for Measuring Hydraulic Fracturing Efficiency by Utilizing the Real-Time Treatment Data. In Proceedings of the International Petroleum Technology Conference, Riyadh, Saudi Arabia, 21–23 February 2022; p. D031S107R002. [CrossRef]
128. Blauer, R.E.; Holcomb, D.L. Using 3D fracture simulation alone may result in incorrect fracture-geometry determination and unreliable real-time fracture analysis. In Proceedings of the SPE Annual Technical Conference and Exhibition, Denver, CO, USA, 6–9 October 1996; p. SPE-36674. [CrossRef]
129. Dung, N.; David, C.; Tom, D.; Jon, S.; Nico, R.; Annie, O. Practical applications of water hammer analysis from hydraulic fracturing treatments. In Proceedings of the SPE Hydraulic Fracturing Technology Conference and Exhibition, Virtual, 4–6 May 2021; p. D011S002R009. [CrossRef]
130. Carey, M.A.; Mondal, S.; Sharma, M.M. Analysis of water hammer signatures for fracture diagnostics. In Proceedings of the SPE Annual Technical Conference and Exhibition, Houston, TX, USA, 28–30 September 2015; p. D031S034R003. [CrossRef]
131. Holzhausen, G.; Gooch, R. Impedance of hydraulic fractures: Its measurement and use for estimating fracture closure pressure and dimensions: Presented at the SPE. In Proceedings of the DOE Low Permeability Gas Reservoirs Symposium, Denver, CO, USA, 19–22 May 1985. [CrossRef]
132. Paige, R.W.; Murray, L.R.; Roberts, J.D.M. Field application of hydraulic impedance testing for fracture measurement. *SPE Prod. Facil.* **1995**, *10*, 7–12. [CrossRef]
133. Yew, C.H.; Ashour, A.A.I.S. A Study of the Fracture Impedance Method. In Proceedings of the Annual Technical Meeting, Calgary, AB, Canada, 9–11 June 1996. [CrossRef]
134. Patzek, T.W.; De, A. Lossy transmission line model of hydrofractured well dynamics. In Proceedings of the SPE Western Regional Meeting, Bakersfield, CA, USA, 10–13 May 1998; p. SPE-46195. [CrossRef]
135. Mondal, S. Pressure Transients In Wellbores: Water Hammer Effects And Implications For Fracture Diagnostics Diagnostics. Master's Thesis, The University of Texas at Austin, Austin, TX, USA, December 2010.
136. Carey, M.A.; Mondal, S.; Sharma, M.M.; Hebert, D.B. Correlating water hammer signatures with production log and microseismic data in fractured horizontal wells. In Proceedings of the SPE Hydraulic Fracturing Technology Conference and Exhibition, The Woodlands, TX, USA, 9–11 February 2016; p. D021S004R006. [CrossRef]
137. Iriarte, J.; Merritt, J.; Kreyche, B. Using water hammer characteristics as a fracture treatment diagnostic. In Proceedings of the SPE Oklahoma City Oil and Gas Symposium/Production and Operations Symposium, Oklahoma City, OK, USA, 27–31 March 2017; p. D031S007R004. [CrossRef]
138. Shen, J.; He, H.; Li, Y.; Zou, L.; Wang, Y.; Zhu, Z.; Fu, S. An investigation of data analysis method for hydraulic fracturing based on the water hammer effect. *Unconv. Resour.* **2023**, *3*, 284–290. [CrossRef]
139. Hu, X.; Luo, Y.; Zhou, F.; Qiu, Y.; Li, Z.; Li, Y. Evaluation of multi-fractures geometry based on water hammer signals: A new comprehensive model and field application. *J. Hydrol.* **2022**, *612*, 128240. [CrossRef]
140. Jia, K.; Wang, X.; Lu, D. Comprehensive model for multi-fracture localization based on water hammer signals: Evaluation and field application. *Phys. Fluids* **2024**, *36*, 123612. [CrossRef]
141. Castillo, J.L. Modified fracture pressure decline analysis including pressure-dependent leak off. In Proceedings of the SPE Rocky Mountain Petroleum Technology Conference/Low-Permeability Reservoirs Symposium, Denver, CO, USA, 18–19 May 1987; p. SPE-16417. [CrossRef]
142. Yuan, X.; Zhang, Y.; Liu, J.; Peng, F.; Teng, Q.; Xiao, Y.; Han, X. A method of quickly evaluating the fracture complexity of network fracturing. In Proceedings of the International Petroleum Technology Conference, Bangkok, Thailand, 14–16 November 2016; p. D011S011R006. [CrossRef]

143. Tu, Z.; Hu, X.; Zhou, F.; Huang, G.; Han, S.; Zhou, Q. A new multi-fracture geometry inversion model based on hydraulic-fracture treatment pressure falloff data. *J. Pet. Sci. Eng.* **2022**, *215*, 110724. [CrossRef]
144. Jatykov, T.; Bimuratkyzy, K. Case study: An approach for hydraulic fracturing minifrac G-function analysis in relation to facies distribution in multilayered clastic reservoirs. *SPE Prod. Oper.* **2022**, *37*, 99–106. [CrossRef]
145. Kolle, J.J.; Theimer, A.R.; Fraser, A.W.; Fletcher, S. Predicting the extended reach capabilities of a water-hammer tool with variable bypass control. In Proceedings of the SPE/ICoTA Well Intervention Conference and Exhibition, Houston, TX, USA, 22–23 March 2016; p. D021S008R004. [CrossRef]
146. Ma, X.; Zhou, F.; Ortega Andrade, J.A.; Gosavi, S.; Burch, D. Evaluation of water hammer analysis as diagnostic tool for hydraulic fracturing. In Proceedings of the SPE/AAPG/SEG Unconventional Resources Technology Conference, Denver, CO, USA, 22–24 July 2019; p. D023S030R007. [CrossRef]
147. Bakar, R.; Ozkan, E.; Kazemi, H. Modeling and analysis of diagnostic fracture injection tests DFITs. In Proceedings of the SPE Europec featured at EAGE Conference and Exhibition, Amsterdam, The Netherlands, 18–21 October 2021; p. D031S006R001. [CrossRef]
148. Wenchao, L.; Chengcheng, Q.; Ping, W.; Wensong, H.; Yuewu, L.; Wei, D.; Yuping, S. Study on fracture characteristics difference between fracturing fluid flowback and gas production stages of shale gas wells. *Chin. J. Theor. Appl. Mech.* **2023**, *55*, 1382–1393. [CrossRef]
149. Song, B.; Ehlig-Economides, C.; Economides, M.J. Design of multiple transverse fracture horizontal wells in shale gas reservoirs. In Proceedings of the SPE Hydraulic Fracturing Technology Conference and Exhibition, The Woodlands, TX, USA, 24–26 January 2011; p. SPE-140555. [CrossRef]
150. Taghavinejad, A.; Sharifi, M.; Heidaryan, E.; Liu, K.; Ostadhassan, M. Flow modeling in shale gas reservoirs: A comprehensive review. *J. Nat. Gas Sci. Eng.* **2020**, *83*, 103535. [CrossRef]
151. Crafton, J.W. Well evaluation using early time post-stimulation flowback data. In Proceedings of the SPE Annual Technical Conference and Exhibition, New Orleans, LA, USA, 27–30 September 1998; p. SPE-49223. [CrossRef]
152. Crafton, J.W.; Gunderson, D. Use of extremely high time-resolution production data to characterize hydraulic fracture properties. In Proceedings of the SPE Annual Technical Conference and Exhibition, San Antonio, TX, USA, 24–27 September 2006; p. SPE-103591. [CrossRef]
153. Clarkson, C.R.; Williams-Kovacs, J.D. Modeling two-phase flowback of multifractured horizontal wells completed in shale. *Spe J.* **2013**, *18*, 795–812. [CrossRef]
154. Xu, Y.; Adefidipe, O.A.; Dehghanpour, H. Estimating fracture volume using flowback data from the Horn River Basin: A material balance approach. *J. Nat. Gas Sci. Eng.* **2015**, *25*, 253–270. [CrossRef]
155. Williams-Kovacs, J.D.; Clarkson, C.R. A modified approach for modeling two-phase flowback from multi-fractured horizontal shale gas wells. *J. Nat. Gas Sci. Eng.* **2016**, *30*, 127–147. [CrossRef]
156. Wang, F.; Pan, Z.; Zhang, S. Impact of chemical osmosis on water leak off and flowback behavior from hydraulically fractured gas shale. *J. Pet. Sci. Eng.* **2017**, *151*, 264–274. [CrossRef]
157. Xu, Y.; Dehghanpour, H.; Ezulike, O.; Virues, C. Effectiveness and time variation of induced fracture volume: Lessons from water flowback analysis. *Fuel* **2017**, *210*, 844–858. [CrossRef]
158. Yang, T.; Wu, X. Water flowback analysis and hydraulic fracture characterization in Marcellus unconventional reservoir. In Proceedings of the SPE Oklahoma City Oil and Gas Symposium/Production and Operations Symposium, Oklahoma City, OK, USA, 27–31 March 2017; p. D031S009R002. [CrossRef]
159. Zhang, F.; Emami-Meybodi, H. A semianalytical method for two-phase flowback rate-transient analysis in shale gas reservoirs. *SPE J.* **2020**, *25*, 1599–1622. [CrossRef]
160. Zhang, F.; Emami-Meybodi, H. A type-curve method for two-phase flowback analysis in hydraulically fractured hydrocarbon reservoirs. *J. Pet. Sci. Eng.* **2022**, *209*, 109912. [CrossRef]
161. Lee, S.T.; Brockenbrough, J.R. A new approximate analytic solution for finite-conductivity vertical fractures. *SPE Form. Eval.* **1986**, *1*, 75–88. [CrossRef]
162. Brown, M.L.; Ozkan, E.; Raghavan, R.S.; Kazemi, H. Practical Solutions for Pressure-Transient Responses of Fractured Horizontal Wells in Unconventional Shale Reservoirs. *SPE Reserv. Eval. Eng.* **2009**, *14*, 663–676. [CrossRef]
163. Stalgorova, E.; Mattar, L. Practical analytical model to simulate production of horizontal wells with branch fractures. In Proceedings of the SPE Canadian Unconventional Resources Conference, Calgary, AB, Canada, 30 October 2012. [CrossRef]
164. Zhao, Y.; Zhang, L.; Zhao, J.; Luo, J.-X.; Zhang, B.-N. "Triple porosity" modeling of transient well test and rate decline analysis for multi-fractured horizontal well in shale gas reservoirs. *J. Pet. Sci. Eng.* **2013**, *110*, 253–262. [CrossRef]
165. Qiu, K.; Li, H. A new analytical solution of the triple-porosity model for history matching and performance forecasting in unconventional oil reservoirs. *SPE J.* **2018**, *23*, 2060–2079. [CrossRef]
166. Meng, M.; Chen, Z.; Liao, X.; Wang, J.; Shi, L. A well-testing method for parameter evaluation of multiple fractured horizontal wells with non-uniform fractures in shale oil reservoirs. *Adv. Geo-Energy Res.* **2020**, *4*, 187–198. [CrossRef]

167. Wang, Y.; Liu, H.; Hu, X.; Dai, C.; Fang, S. Fracture network types revealed by well test curves for shale reservoirs in the Sichuan Basin, China. *Energy Geosci.* **2024**, *5*, 100135. [CrossRef]
168. Ezulike, D.O.; Dehghanpour, H. A model for simultaneous matrix depletion into natural and hydraulic fracture networks. *J. Nat. Gas Sci. Eng.* **2014**, *16*, 57–69. [CrossRef]
169. Stalgorova, K.; Mattar, L. Analytical model for unconventional multifractured composite systems. *SPE Reserv. Eval. Eng.* **2013**, *16*, 246–256. [CrossRef]
170. Deng, Q.; Nie, R.S.; Jia, Y.L.; Huang, X.-Y.; Li, J.-M.; Li, H.-K. A new analytical model for non-uniformly distributed multi-fractured system in shale gas reservoirs. *J. Nat. Gas Sci. Eng.* **2015**, *27*, 719–737. [CrossRef]
171. Zeng, J.; Wang, X.; Guo, J.; Zeng, F. Composite linear flow model for multi-fractured horizontal wells in heterogeneous shale reservoir. *J. Nat. Gas Sci. Eng.* **2017**, *38*, 527–548. [CrossRef]
172. Wu, Y.H.; Fang, S.D.; Wang, S.R.; Huang, S.J.; Ma, L.Q.; Fu, G.Q. A novel production data analysis method for multi-fractured horizontal wells with infill well-caused fracture interference. *Pet. Sci.* **2023**, *20*, 2967–2980. [CrossRef]
173. Cheng, L.-S.; Cao, C.; Pan, Q.-Y.; Jia, P.; Cao, R.-Y.; Wang, Z.-K.; Shi, J.-J. A semi-analytical pressure and rate transient analysis model for inner boundary and propped fractures exhibiting dynamic behavior under long-term production conditions. *Pet. Sci.* **2024**, *21*, 2520–2535. [CrossRef]
174. Chen, Z.; Liao, X.; Zhao, X.; Dou, X.; Zhu, L. Performance of horizontal wells with fracture networks in shale gas formation. *J. Pet. Sci. Eng.* **2015**, *133*, 646–664. [CrossRef]
175. Li, Z.; Wu, X.; Han, G.; Zhang, L.; Zhao, R.; Shi, S. A semi-analytical pressure model of horizontal well with complex networks in heterogeneous reservoirs. *J. Pet. Sci. Eng.* **2021**, *202*, 108511. [CrossRef]
176. Cui, G.; Tan, Y.; Chen, T.; Feng, X.-T.; Elsworth, D.; Pan, Z.; Wang, C. Multidomain two-phase flow model to study the impacts of hydraulic fracturing on shale gas production. *Energy Fuels* **2020**, *34*, 4273–4288. [CrossRef]
177. Deng, J.; He, J.; Song, H. An improved mathematical model of gas-water two-phase flows in fractured horizontal wells accounting for physical contact behaviors of fractures with total factor characteristics. *Phys. Fluids* **2024**, *36*, 8. [CrossRef]
178. Clarkson, C.R.; Haghshenas, B.; Ghanizadeh, A.; Qanbari, F.; Williams-Kovacs, J.D.; Riazi, N.; Deglint, H.J. Nanopores to megafractures: Current challenges and methods for shale gas reservoir and hydraulic fracture characterization. *J. Nat. Gas Sci. Eng.* **2016**, *31*, 612–657. [CrossRef]
179. Alfarge, D.; Wei, M.; Bai, B. Evaluating the performance of hydraulic-fractures in unconventional reservoirs using production data: Comprehensive review. *J. Nat. Gas Sci. Eng.* **2019**, *61*, 133–141. [CrossRef]
180. Barree, R.D.; Fisher, M.K.; Woodroof, R.A. A practical guide to hydraulic fracture diagnostic technologies. In Proceedings of the SPE Annual Technical Conference and Exhibition, San Antonio, TX, USA, 29 September 2002; p. SPE-77442. [CrossRef]
181. Cipolla, C.L.; Wright, C.A. State-of-the-art in hydraulic fracture diagnostics. In Proceedings of the SPE Asia Pacific Oil and Gas Conference and Exhibition, Brisbane, Australia, 16–18 October 2000; p. SPE-64434. [CrossRef]
182. Wright, C.A.; Cipolla, C.C. Diagnostic Techniques to Understand Hydraulic Fracturing: What? Why? and How? In Proceedings of the SPE/CERI Gas Technology Symposium, Calgary, AB, Canada, 3–5 April 2000; p. SPE-59735-MS. [CrossRef]
183. Clarkson, C.R.; Beierle, J.J. Integration of microseismic and other post-fracture surveillance with production analysis: A tight gas study. *J. Nat. Gas Sci. Eng.* **2011**, *3*, 382–401. [CrossRef]
184. Holley, E.H.; Zimmer, U.; Mayerhofer, M.J.; Samson, E. Integrated analysis combining microseismic mapping and fiber-optic distributed temperature sensing (DTS). In Proceedings of the SPE Canada Unconventional Resources Conference, Calgary, AB, Canada, 19–21 October 2010; p. SPE-136565. [CrossRef]

Disclaimer/Publisher's Note: The statements, opinions and data contained in all publications are solely those of the individual author(s) and contributor(s) and not of MDPI and/or the editor(s). MDPI and/or the editor(s) disclaim responsibility for any injury to people or property resulting from any ideas, methods, instructions or products referred to in the content.